Aus der Berufsgenossenschaftlichen Unfallklinik

Klinik für Unfall- und Wiederherstellungschirurgie an der
Universität Tübingen

Magnesium supplementation reduces cigarette smoke–associated cell damage in 3D bone fracture healing model

Inaugural -Dissertation
zur Erlangung des Doktorgrades
der Medizin

der Medizinischen Fakultät
der Eberhard Karls Universität
zu Tübingen

vorgelegt von

Weng, Weidong

2022

Dekan: Professor Dr. B. Pichler

1. Berichterstatter: Professor Dr. A. Nüssler
2. Berichterstatter: Professor Dr. M. Held

Tag der Disputation: 11.07.2022

To my parents

Table of contents

List of Figures

List of Tables

List of abbreviations

AP	Alkaline phosphatase
BMP-2	Bone morphogenic protein-2
BMP-4	Bone morphogenic protein-4
BMP-7	Bone morphogenic protein-7
BSA	Bovine serum albumin
$CaCl_2$	Calcium chloride
CA II	Carbonic anhydrase II
CSE	Cigarette smoke extract
CS	Cigarette smoking
DMSO	Dimethylsulfoxide
DPBS	Dulbecco's Phosphate Buffered Saline
EtOH	Ethanol
FBS	Fetal bovine serum
GEL	Gelatin
HCl	Hydrogen chloride
IL-1	Interleukin 1
IL-8	Interleukin 1
M-CSF	Macrophage colony-stimulating factor
Mg	Magnesium
$MgCl_2$	Magnesium chloride
MSCs	Marrow mesenchymal stem cells
MMP-9	Matrix metalloproteinase-9
MEM α	Minimum Essential Medium Eagle alpha
OCN	Osteocalcin
OPG	Osteoprotegerin
pNPP	Para- Nitropheyl-Phosphate
PMA	Phorbole-12-myristate-13-acetate
PBS	Phosphate buffered saline
PINP	Procollagen type I N-terminal propeptide
RANKL	Receptor activator of nuclear factor kappa-B ligand
SDS	Sodium Dodecyl Sulfate
NaOH	Sodium hydroxide
NaCl	Sodiumchloride

SRB	Sulforhodamine B
TRAP	Tartrate-resistant acid phosphatase
TEMED	Tetramethylethylenediamine
3D	Three dimensional
2D	Two dimensional

Chapter 1

1. Introduction

1.1. Bone

Bone is a complex multifunctional organ and exerts a crucial role in not only offering mechanical and structural support to protect the vital organs but also regulating endocrine metabolism (Filippi *et al.*, 2020). This organ is generally structured with two major aspects: extracellular matrix and cells (Figure 1.1) (Nijweide *et al.*, 1986, Xu *et al.*, 2019). Bone components, structure, and function are influenced by multiple factors, including age, concomitant diseases, and an unhealthy lifestyle (*e.g.*, smoking) (Murray *et al.*, 2013, Bahney *et al.*, 2015). Alterations in bone components have the potential to affect the development and growth of bone-related cells, which may further influence the quality and integrity of bone tissue (Murray *et al.*, 2013, Bahney *et al.*, 2015). Understanding and characterizing bone cells interactions in detail is believed to be critical to guiding suitable further treatments (Ghiasi *et al.*, 2017).

1.1.1. Extracellular matrix

Bone extracellular matrix, a complex three-dimensional (3D) structure (Hynes, 2009), exerts a crucial role in mechanical and structural support to modulate complex cellular activities such as cell migration, proliferation, and differentiation (Gentili and Cancedda, 2009, Alford *et al.*, 2015, Weng *et al.*, 2021). The matrix is structured with organic and inorganic phases (Weng *et al.*, 2021). Type I collagen, the most abundant organic substance in bone tissue, has been shown to induce osteoclastic differentiation of monocytes and osteoblastic differentiation of MSCs (Elango *et al.*, 2019, Weng *et al.*, 2021). Calcium phosphate and hydroxyapatite, the major inorganic components in bone tissue, also possess the ability to regulate the differentiation of bone-forming cells (Liu *et al.*, 2007) and bone-resorbing cells (Maria *et al.*, 2014). When both organic and inorganic components are present simultaneously, the progression and development of bone-related cells are well regulated (Weng *et al.*, 2021). For example, the expression of *annexin A8* on bone precursor cells required for osteoclastic differentiation is

observed only when both organic and inorganic components co-exist (Crotti *et al.*, 2011). Thus, an effective and valid study *in vitro* platform has to incorporate organic and inorganic components from bone tissue, like collagen and hydroxyapatite, to generate a bone cell culture system with features comparable to those seen *in vivo*.

1.1.2. Cells

Bone tissue consists of several cell types, which are mainly divided into bone-forming cells (Karsenty and Wagner, 2002) and bone-resorbing cells (Hadjidakis and Androulakis, 2006). These two categories of cells are engaged in osteogenic and osteoclastic differentiation and exert a crucial role in the maintenance of bone metabolism (Kular *et al.*, 2012).

Osteoblasts represent a species of bone-forming cells, comprising approximately 5% of all bone-related cells from bone tissue (Ohgushi *et al.*, 2003). This kind of cell originates from bone marrow mesenchymal stem cells (MSCs). Throughout osteogenesis, MSCs undergo into pre-osteoblasts that give rise to osteoblasts and eventually turn into osteocytes (Infante and Rodriguez, 2018). Osteogenic differentiation and bone forming cells function are controlled *via* numerous factors and molecules, like Notch ligands (Regan and Long, 2013, Fei *et al.*, 2015), Wnt ligands (Westendorf *et al.*, 2004, Krishnan *et al.*, 2006), bone morphogenetic proteins (Rosen, 2006, Toprak *et al.*, 2021), transforming growth factors (Esposito *et al.*, 2021, Berglund *et al.*, 2021), and so on.

Osteoclasts are multinuclear cells with bone resorption activity derived from hematopoietic stem cells (Clézardin *et al.*, 2021). Osteoclastogenesis is a complicated process through which monocytes give rise to mononuclear pre-osteoclasts and fuse with each other to form multinuclear giant cells with bone resorption properties (Teitelbaum, 2000). Osteoclastic differentiation and function are mainly controlled *via* two molecules, macrophage colony-stimulating factor (M-CSF) (Zaidi, 2007) and receptor activator of nuclear kappa-B ligand (RANKL) (Hodge *et al.*, 2011).

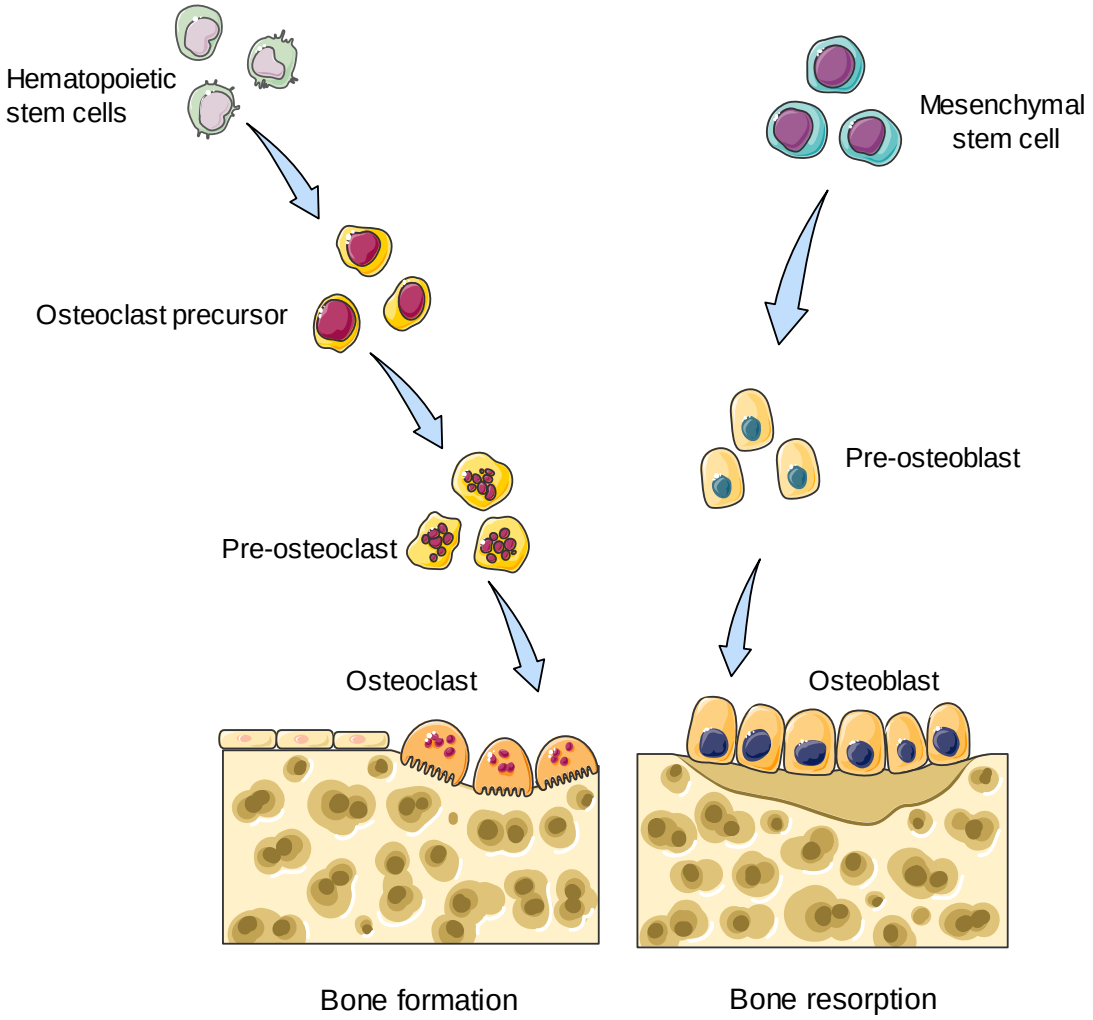

Figure 1.1 Types and development of bone-related cells. The image was generated with the assistance of Servier Medical Art (https://smart.servier.com/).

1.2. Bone fracture healing

Bone fractures are frequently encountered in orthopedic departments (Bian *et al.*, 2018). Despite appropriate treatment methods, 10% of fractures result in impaired fracture healing (Buza and Einhorn, 2016). The treatment of delayed union or nonunion fracture healing is a complex process, associated with an extended recovery period and length of hospital stay and increased medical expenses (Gomez-Barrena *et al.*, 2015). In Europe, it is estimated that the cost for treating patients suffering from orthopedic diseases is appropriately 10% of total medical expense, of which most expenditure is incurred by multiple surgical interventions after delayed union or nonunion fracture healing (Ehnert *et al.*, 2020). Understanding and characterizing the role of bone cells in

bone fracture healing in detail is believed to be critical to guiding suitable further treatments (Ghiasi *et al.*, 2017).

Bone fracture healing is a developmental process of overlapping, consecutive phases in which fractured bones are restored to their pre-fracture state after an injury. This process consists of three phases, beginning with an inflammatory phase, followed by a reparative phase, and ending with a remodeling phase (Figure 1.2) (Schindeler *et al.*, 2008, Mehta *et al.*, 2012).

1.2.1. Bone fracture healing – inflammatory phase

Following bone trauma or fracture, the bone tissue integrity and vascular system are drastically altered (Kon *et al.*, 2001). Several cell types (monocytes, macrophages, B cells, T cells, MSCs, *etc.*) from the vascular system and bone marrow aggregate in the injured region, contributing to the formation of a fracture hematoma (Sheen and Garla, 2021). The hematoma represents a fibrin network for the attachment and migration of cells, and exerts critical functions in the initiation and development of molecular and cellular events required for successful fracture healing (Kolar *et al.*, 2011). The inflammatory phase of bone fracture healing shows a remarkable elevation in the pro-inflammatory cytokines interleukin 1 (IL-1) (Wang *et al.*, 2016) and IL-6 (Cho *et al.*, 2007), attracting massive inflammatory cells into the fracture hematoma (Claes *et al.*, 2012). Additionally, the hematoma microenvironment has a low pH and low oxygen content, enhancing the ability of macrophages to clear apoptotic and necrotic cells and subsequently triggering the regeneration phase *via* the release of pro-angiogenic factors (vascular endothelial growth factor, platelet-derived growth factor, IL-8, *etc.*) (Andrew *et al.*, 1995, Bouletreau *et al.*, 2002, Nanko *et al.*, 2009) and osteogenic factors (bone morphogenic protein [BMP]-2, BMP-4, BMP-7) (Bostrom *et al.*, 1995, Lissenberg-Thunnissen *et al.*, 2011). These secreted factors are potentially conducive to the migration, proliferation, differentiation, and metabolism of multipotent stem cells from the bone marrow (Granero-Molto *et al.*, 2009). Moreover, these cells are capable of differentiating into numerous cell lineages including osteoblasts, fibroblasts, angioblasts, and chondrocytes, facilitating the development and progression of

osteogenesis and angiogenesis in the injured region (Pittenger *et al.*, 1999). The inflammatory process is commonly rapid, taking from several days to 14 days (Wang and Yeung, 2017).

1.2.2. Bone fracture healing – reparative phase

In the reparative phase, endochondral and intramembranous ossification are the two main processes, contributing to bone regeneration at the fracture site (Ortega *et al.*, 2004). Endochondral ossification is a complex, multi-stage process. MSCs differentiate into chondrocytes that are able to secrete the cartilage extracellular matrix, facilitating the formation of cartilaginous callus (Zhou *et al.*, 2014). This soft tissue may increase in size and content over time, resulting in the disruption of blood flow to newly generated tissue and increased tissue tension (Fang *et al.*, 2005). The resulting hypoxic microenvironment constrains osteoblastogenesis and bone formation, while chondrocytes can proliferate and differentiate in environment. Afterwards, chondrocytes turn into hypertrophic chondrocytes, secrete cartilage extracellular matrix, and ultimately undergo apoptosis (Provot and Schipani, 2005). With the decrease in tissue tension at the fracture site, blood vessels invade the cartilage extracellular matrix, bringing osteoclasts and MSCs to initiate the resorption of cartilage extracellular matrix and the formation of bone extracellular matrix (Yang *et al.*, 2014). As osteogenesis and mineralization of MSCs progress, the soft bone tissue turns firm and hard at the fracture site. Intramembranous ossification generally takes place in woven bone tissue through the direct differentiation of MSCs into bone-forming cells in the absence of cartilage formation as an intermediate stage (Xian *et al.*, 2004). These two processes of ossification are involved in the reparative phase, taking from 2 to 6 weeks (Wang and Yeung, 2017).

1.2.3. Bone fracture healing – remodeling phase

The last step in bone fracture healing is the remodeling phase in which woven bone callus is turned into lamellar bone (Szczesny, 2002, Schindeler *et al.*, 2008). Bone-resorbing cells adhere to the fracture site and release acid and osteoclast-related factors

like cathepsin K (Fujita *et al.*, 2013, Walia *et al.*, 2018) and matrix metalloproteinase-9 (MMP-9) (Engsig *et al.*, 2000, Christensen and Shastri, 2015), forming small pits or resorption cavities to resorb woven bone tissue. Simultaneously, bone-forming cells adhere to these pits and deposit minerals and organic compounds (Sims and Gooi, 2008). These two processes maintain a dynamic balance of production and removal of the fractured bone tissue, preserving the bone's mechanical strength and mass. The bone remodeling phase also takes place in healthy bone tissue, keeping a suitable degree of bone metabolism, which is comparable to bone fracture healing in patients following trauma (Karsenty, 2000). This final phase takes from 8 weeks to 2 years (Wang and Yeung, 2017).

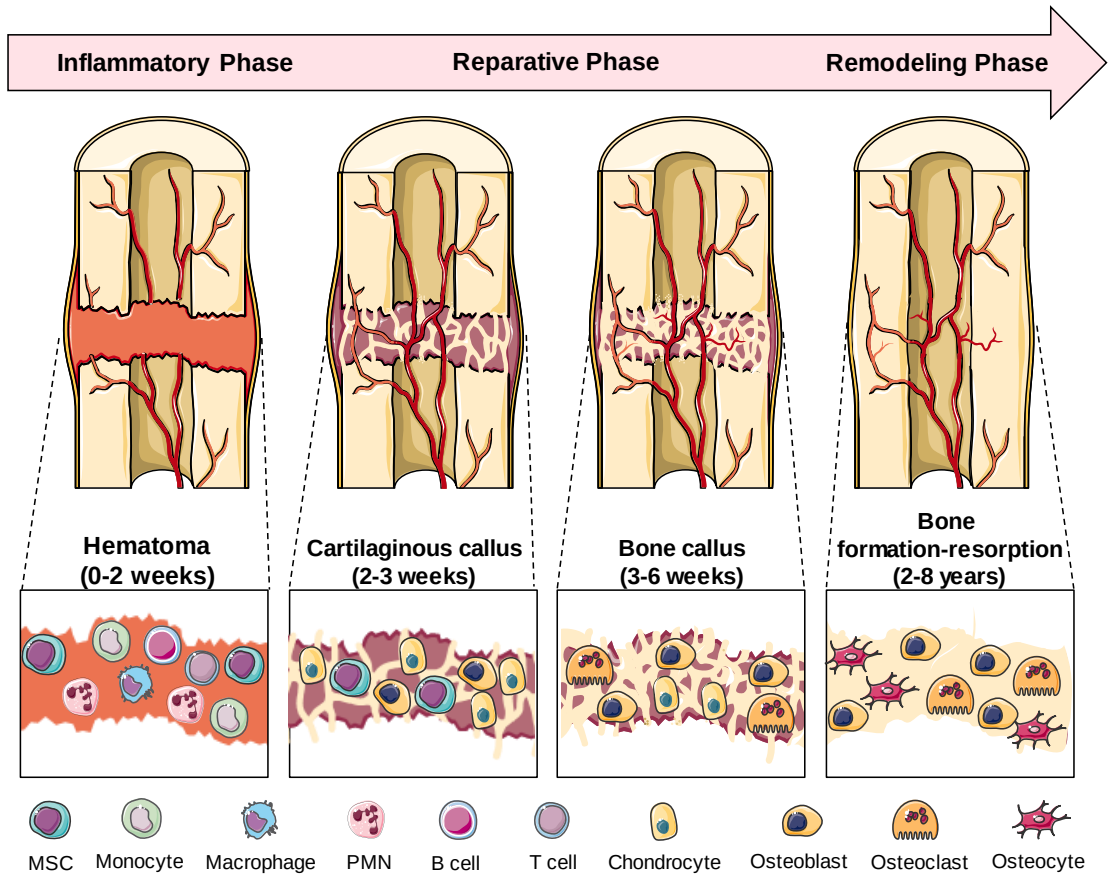

Figure 1.2 The phases of bone fracture healing. Bone fracture healing is a developmental process involving three phases: inflammatory, reparative, and remodeling. The image was generated with the assistance of Servier Medical Art (https://smart.servier.com/).

1.2.4. Bone fracture healing – *in vitro* models

Currently, animal models are predominantly used to study bone fracture healing (Ehnert *et al.*, 2020). It is worth noting that animal models have several shortcomings. Bones in the animal models undergoing stress are not the same as human bone tissue because of the quadruped posture (Ehnert *et al.*, 2020). Descriptions of impaired fracture healing seem to be not well-defined in animal models. Furthermore, the ethical implications of animal experiments should be taken into account. Hence, there has become a pressing need for a stable and effective *in vitro* model, simulating the bone fracture healing.

For this, we chose SCP-1 cells (MSCs) and THP-1 cells (osteoclast precursor cells) as our experimental cells. It has been shown that osteogenic differentiation of SCP-1 cells and osteoclastic differentiation of THP-1 cells are implicated as osteogenesis or osteoclastogenesis in the reparative phase, respectively (Ehnert *et al.*, 2020, Weng *et al.*, 2021). SCP-1 cells are capable of releasing crucial cytokines required for osteoclastic differentiation of THP-1 cells, like RANKL and M-CSF (Ehnert *et al.*, 2020, Weng *et al.*, 2021). Aside from cell–cell interactions, cell–matrix interactions have to be taken into account to guarantee a cell culture model which can accurately reflect the complex cellular events during fracture healing (Ehnert *et al.*, 2020, Weng *et al.*, 2021). Scaffolds have been used as promising materials for the differentiation of osteoblast- and osteoclast-like cells, like MSCs and osteoclast precursor cells (Nair *et al.*, 2015, Panzavolta *et al.*, 2018). It has been reported that the scaffold comprises organic (gelatin) and inorganic phases (hydroxyapatite), realistically mimicking the *in vivo* bone microenvironment (Weng *et al.*, 2020). However, the key to achieving a reliable, reproducible, and valid cell culture model lies in preserving the cell function and viability of these two cell lines directly cultured on the scaffolds. There are two major cultivation conditions that need to be optimized: the medium and the appropriate seeding proportion of SCP-1 and THP-1 cells.

1.3. Consumption of tobacco cigarettes

Tobacco consumption represents one of the most common risk factors affecting progression of diseases across the world (Yaragani *et al.*, 2020, Aspera-Werz *et al.*,

2020). As reported by the World Health Organization, tobacco consumption is responsible for nearly 6.5 million deaths per year throughout the world (Soares do Amaral *et al.*, 2016). Moreover, it estimates that there will be approximately 8 million deaths per year attributed to tobacco consumption throughout the world by 2050 (Soares do Amaral *et al.*, 2016). The most commonly accepted approach to consuming tobacco is cigarette smoking (CS) (Nemmar *et al.*, 2020). CS has obvious detrimental effects on health outcomes, which correlate with long-lasting diseases such as osteoporosis (Aspera-Werz *et al.*, 2018, Ratajczak *et al.*, 2021), delayed or nonunion fracture healing (Nishino *et al.*, 2021, Ryan *et al.*, 2021), diabetes (Lecka-Czernik, 2017, Marin *et al.*, 2018), lung diseases (Rahal *et al.*, 2017, O'Keeffe *et al.*, 2018). Cigarette smoke contains a minimum of 6500 molecular species, with approximately 2.3% of these compounds recognized as harmful or poisonous to human health (Velilla *et al.*, 2013). Nicotine is known to be the primary addictive ingredient in a conventional tobacco cigarette. When a cigarette is smoked, nicotine initially enters the pulmonary system, then the cardiovascular system, and in a very short time (approximately 17 s) the central system (brain) (Benowitz, 2008), where it exerts crucial roles in the addiction process. Fast distribution to the brain is regarded to exert a crucial role in the high abuse/dependence liability of nicotine inhalation in comparison to the other approaches to nicotine administration such as nicotine nasal sprays, patches, and gums. (Prochaska and Benowitz, 2019). Additionally, it has been demonstrated that other compounds in the cigarette smoke favor the high abuse/dependence liability of nicotine, including several ingredients that directly or indirectly inhibit monoamine oxidase (Lewis *et al.*, 2007, van der Toorn *et al.*, 2019), as well as some enzymes that directly or indirectly degrade neurotransmitters (Prochaska and Benowitz, 2019, Li *et al.*, 2020).

1.4. Cigarette smoking and bone

Numerous studies have revealed the adverse impacts of CS on the musculoskeletal system *in vitro* and *in vivo* (Figure 1.3) (Aspera-Werz *et al.*, 2018, Ehnert *et al.*, 2019, Reumann *et al.*, 2020). In a clinical trial, researchers showed that heavy smokers had a substantially greater risk of prolonged hospitalization and complications after total joint

replacement, compared to nonsmokers (Tischler *et al.*, 2017, Sahota *et al.*, 2018, Ehnert *et al.*, 2019). Several animal experiments have revealed that long-term exposure to cigarette smoke contributes to the reduction of bone mass and bone strength (Akhter *et al.*, 2003, Reumann *et al.*, 2020). Furthermore, a recent *in vitro* experiment revealed that chronic exposure to cigarette smoke extract (CSE) upregulated osteoclastic function and downregulated osteoblastic function in a bone cell culture model, contributing to an osteoporotic microenvironment (Zhu *et al.*, 2020).

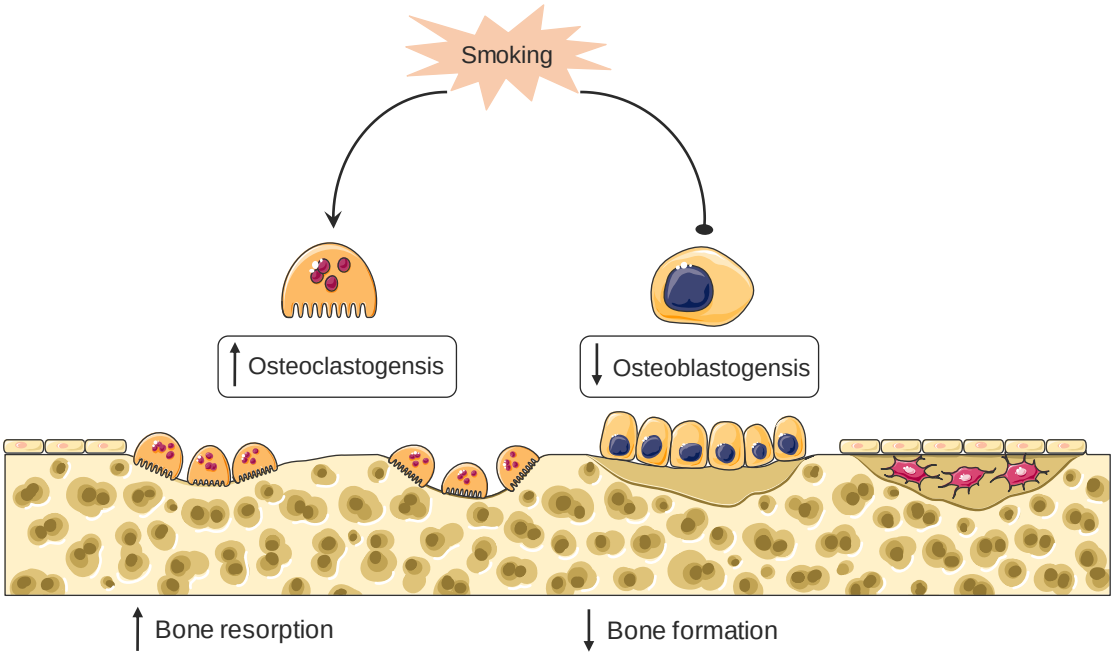

Figure 1.3 The role of CS in bone metabolism. Chronic exposure to cigarette smoke upregulates osteoclastic function and downregulates osteoblastic function in bone cells, contributing to an osteoporotic microenvironment. The image was generated with the assistance of Servier Medical Art (https://smart.servier.com/).

1.5. Magnesium: a cofactor in low serum levels on smokers

Magnesium (Mg), a crucial cofactor, is engaged in approximately 350 metabolic activities like energy metabolism and nucleic acid synthesis (Vernon, 1988, Paolisso *et al.*, 1990, Mieczkowski *et al.*, 2013). Healthy adults possess approximately 24 g of Mg, of which about 50–60% is presented in the bone (Ni *et al.*, 2020). The serum Mg concentration is strictly regulated and maintained within the physiological range of 0.7

to 1 mM (Alhosaini and Leehey, 2015). When the serum Mg concentration is lower than 0.7 mM, the patient is diagnosed with Mg deficiency.

Mg deficiency has been linked to a deterioration in bone micro-architecture and low bone mass and strength (Saito *et al.*, 2004, Mahdavi-Roshan *et al.*, 2015). Several clinical studies have revealed that insufficient Mg intake can decrease blood supply to bones (Warburton *et al.*, 2007) and stimulate the production of inflammatory factors (Mazur *et al.*, 2007), negatively affecting bone quality and quantity (Rude and Gruber, 2004). The absence of Mg intake may trigger osteoporotic-like changes in animal models *via* upregulation of osteoclast activity and downregulation of osteoblast activity (Rude *et al.*, 2003). Interestingly, a clinical study compared serum Mg levels in heavy smokers and nonsmokers and found that heavy smokers had a remarkably lower serum Mg level (0.4 ± 0.1 mM) compared to nonsmokers (1 ± 0.1 mM) (Ata *et al.*, 2015). Therefore, Mg deficiency may be one of the potential reasons why CS can contribute to delayed fracture healing or nonunion fracture healing. Additionally, Mg, a crucial component of human bone mineral, stimulates osteoblast-like cells' survival, proliferation, and osteogenic differentiation, supporting bone growth and formation (Wu *et al.*, 2015, Wang *et al.*, 2017, Lin *et al.*, 2019). Some researchers have revealed that biomaterials rich in Mg can facilitate osteoblast-like cell differentiation and suppress osteoclast-like cell differentiation in *in vitro* cellular experiments and *in vivo* animal studies (Figure 1.4) (Kim *et al.*, 2018, Pinho *et al.*, 2021). In view of this, our subsequent hypothesis is that Mg supplementation may be a possible effective strategy for smokers with osteoporotic bones to improve bone quality.

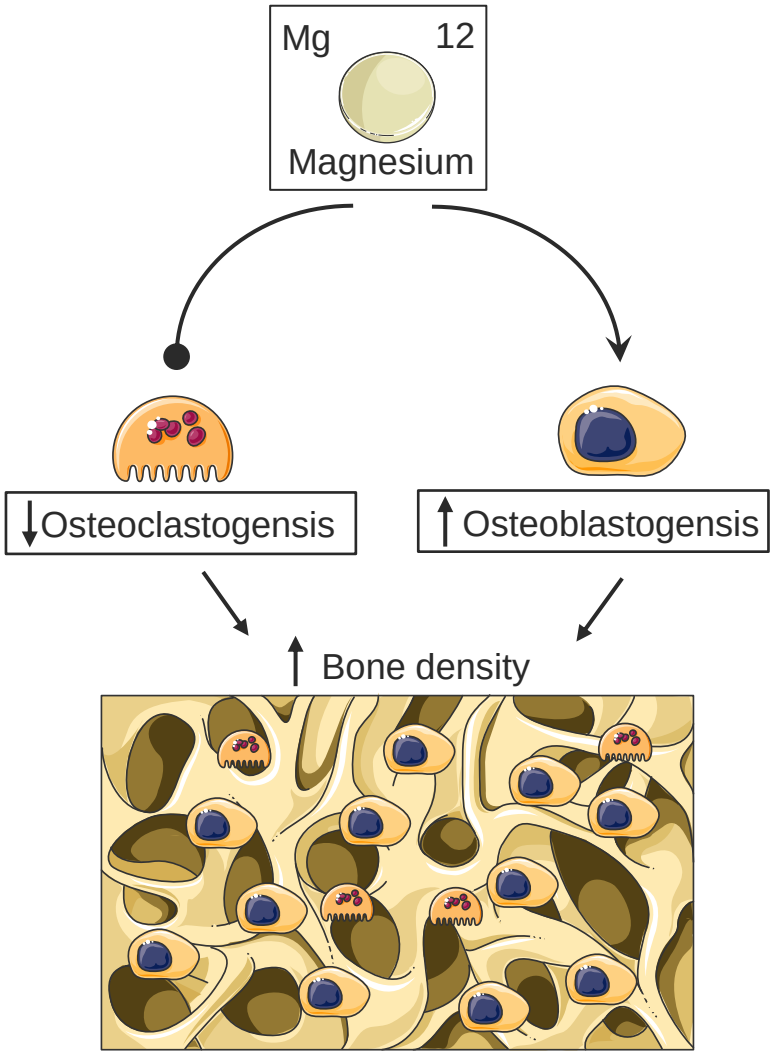

Figure 1.4 The effect of Mg on bone metabolism. Mg possesses the ability to upregulate osteoblastic function and downregulate osteoclastic function in bone cells, contributing to an increase in bone mass. The image was generated with the assistance of Servier Medical Art (https://smart.servier.com/).

1.6. Aim of the research

The intention of this research was to investigate the role of Mg supplementation in a 3D bone co-culture system exposed to CS. To achieve this aim, the following points were addressed:

- Establishment of a 3D bone co-culture model:
  - Physically characterization of the scaffold;
  - Select the appropriate medium to maintain the viability and functionality of SCP-1 and THP-1 cells;
  - Assess the attachment of SCP-1 and THP-1 cells to the scaffold;
  - Optimize the cell ratio to maintain the viability and functionality of SCP-1 and THP-1 cells;
- Evaluate the effects of Mg supplementation on a 3D co-culture system impaired by CS.
- Elucidate the molecular mechanism(s) behind the positive role of Mg supplementation on a 3D co-culture under CS condition.

Chapter 2

2. Materials and Methods

2.1. Materials

2.1.1. Chemicals

Table 2.1: List of used chemicals.

Substance	Article No.	Company
4-Nitrophenol solution 10 mM (pNP)	Sigma	N7660
4-Nitrophenyl acetate (esterase substrate)	Sigma	N8130-5G
4-Nitrophenyl phosphate disodium salt hexahydrate (pNPP)	Carl Roth	4165.1
Acetic acid, purum ≥ 99,0 %	VWR	20104.298
Acrylamide- Bisacrylamide Solution (30%)	Carl Roth	3029.2
Ammonium Persulfate	Carl Roth	9592.2
Brij 35	Carl Roth	CN21.1
Bromophenol	Carl Roth	A152.2
Bromphenol Blue	Carl Roth	A512.2
Calcium chloride	Carl Roth	CN93.1
Calcium chloride ($CaCl_2$)	Carl Roth	CN93.1
Cholecalciferol (Vit.D_3)	Sigma	95230
Dimethylsulfoxide (DMSO)	Carl Roth	4720.2
Dulbecco's Phosphate Buffered Saline (DPBS)	Sigma	D8537
Ethanol (EtOH)	Applichem	A1613
Fetal Bovine Serum (FCS)	Invitrogen	41G7141K
Formaldehyde solution (37 %)	Carl Roth	4979.1
Gelatin	Sigma	G7041
Glutardialdehyd	Carl Roth	3778.1
Glycerin	Carl Roth	7530.1
Glycin	Carl Roth	3908.2
Glycine	Carl Roth	3908.2
HEPES	Carl Roth	HN78.2
Hoechst 33342	Sigma	14533-100MG
Hydrogen chloride (HCl) 4 M	Carl Roth	N076.1
Hydroxyapatite	Sigma	21223
Isopropanol	Honeywell	33539
L-Ascorbic acid-2-phosphate sesqui-magnesium salt	Sigma	A8960-5G
Magnesium chloride ($MgCl_2$)	Carl Roth	KK36.2
MEM α	Thermo Fisher Scientific	22561-054
Methanol	Honeywell	32213
Na_2- Tartrate *2 H_2O	Carl Roth	254.1

Para- Nitropheyl-Phosphate (pNPP)	Carl Roth	4165.1
Phorbole-12-myristate-13-acetate (PMA)	Abcam	AB120297
Resazurin sodium salt	Sigma	199303-1G
RPMI 1640	Sigma	R8758
Sodium Dodecyl Sulfate (SDS)	Carl Roth	CN30.2
Sodium hydroxide (NaOH)	Roth	T135.1
Sodiumacetate	Carl Roth	X891.2
Sodiumchloride (NaCl)	Sigma	S7653
Sulforhodamine B sodium salt	Sigma	S1402-1G
Tetramethylethylenediamine (TEMED)	Carl Roth	2367.3
TRIS	Sigma	T1503- 1KG
TRIS (hydroxymethyl) aminomethan	Carl Roth	AE15.1
Triton-X-100	Carl Roth	3051.2
Trypsin/EDTA	Sigma	T3924
Tween-20	Carl Roth	9127.1
β-Glycerophosphate disodium salt hydrate	Sigma	G9422-10

2.1.2. Solutions

Table 2.2: List of solutions.

Buffers/Mediums/Solutions	Compounds and handling
Acetic acid solution (1%)	500 µl Acetic acid 49.5 ml ddH_2O
AP activity assay buffer	3.75 g Glycine 12.11 g Tris-Base 95.21 mg $MgCl_2$ Adjust volume to 900 ml with ddH_2O Adjust pH to 10.5 with NaOH Adjust volume to 1 l with ddH_2O
AP substrate solution	1.3 mg 4-Nitrophenyl phosphate disodium salt hexahydrate (pNPP) 1 ml AP Activity Assay Buffer (pH 10.5)
APS solution (10%)	2 g Ammonium Persulfate 20 ml ddH_2O
BSA blocking buffer (5%)	0.5 g BSA 50 ml DPBS
Brij 35 solution (1%)	1 g Brij 35 100 ml ddH_2O
CA II substrate buffer	75.7 mg TRIS 219.2 mg NaCl Adjust pH to 7.5 Adjust volume to 50 ml with ddH_2O

CA II activity solution	54.3 mg 4-Nitrophenyl acetate 1.5 ml Ethanol (100%)
Calcein AM stock solution	502 µl DMSO 1 mg Calcein AM
Cholecalciferol stock solution	2 mg Cholecalciferol 10 ml DMSO
Destaining solution	25 ml Methanol 75 ml ddH_2O
Electrophoresis buffer (5X)	75 g Glycine 15.17 g TRIS 5 g SDS Adjust volume to 1 l with ddH_2O
Electrophoresis buffer (1X)	200 ml Electrophoresis buffer 5X 800 ml ddH_2O
Formaldehyde solution (4 %)	12 ml 37 % Formaldehyde solution 88 ml DPBS
Hoechst stock solution	10 mg Hoechst 33342 5 ml DMSO
NaOH solution for DNA quantification	1.25 ml 2 M NaOH solution 48.75 ml ddH_2O
Osteogenic differentiation medium for SCP-1 cells	500 ml MEM α 29 mg L-Ascorbic acid 2-phosphate 0.54 g β-Glycerophosphate 2.98 g HEPES 83 mg Calcium chloride 50 µl Cholecalciferol stock solution 10 ml Fetal bovine serum
Osteogenic differentiation medium for SCP-1/THP-1 co-culture system	250 ml RPMI 1640 250 ml MEM α 29 mg L-Ascorbic acid 2-phosphate 0.54 g β-Glycerophosphate 2.98 g HEPES 83 mg Calcium chloride 50 µl Cholecalciferol stock solution 10 ml Fetal bovine serum
PMA stock solution	1.0 mg Phorbole-12-myristate-13-acetate 8.1 ml DMSO
Resazurin stock solution (11X)	12.5 mg Resazurin sodium salt 50 ml DPBS
Roti- Blue Staining Solution (1X)	20 ml Roti- Blue (5X) 20 ml Methanol 60 ml ddH_2O
SCP-1 cell growing medium	500 ml MEM α 25 ml Fetal bovine Serum

SDS solution (10 %) for zymography	2 g SDS 20 ml ddH_2O
Sulforhodamine B solution	0.2 g Sulforhodamine B Adjust volume to 50 ml with 1 % acetic acid
THP-1 cell growing medium	500 ml RPMI 1640 25 ml Fetal bovine serum
TRIS solution for DNA quantification	6.06 g TRIS 40 ml ddH_2O Adjust pH to 8.0 with HCl Adjust volume to 50 ml with ddH_2O
TRAP - assay buffer	8.2 g Na- Acetate 11.5 g Na_2- Tartrate *2 H_2O 900 ml ddH_2O Adjust pH to 5.5 with HCl Adjust volume to 1 l with ddH_2O
TRAP - substrate buffer solution	1.9 mg pNPP (para-Nitrophenyl-Phosphate) 1ml TRAP- Assay Buffer (pH= 5.5)
TRAP - reaction stop solution	10 ml 2 M NaOH 10 ml ddH_2O
TRIS (1.5 M) for zymography	181.7 g TRIS 900 ml ddH_2O Adjust pH to 8.8 Adjust volume to 1 l with ddH_2O
TRIS (1 M) for zymography	121.1 g TRIS 800 ml ddH_2O Adjust pH to 6.8 Adjust volume to 1 l with ddH_2O
Triton-X-100 solution (0.2%) for immunofluorescence staining	100 µl Triton-X-100 50 ml ddH_2O
Triton-X-100 solution (2.5%) for zymography	25 ml Triton-X-100 1 l ddH_2O
Trypan blue solution	62.5 mg Trypan blue 50 ml Dulbecco's PBS
Zymography developing buffer	6.05 g TRIS 8.766 g NaCl 1.47 g $CaCl_2$ 20 ml 1 % Brij 35 solution Adjust volume to 1 l with ddH_2O
Zymography sample loading buffer (3x)	0.2 g SDS 1 g Glycerin 1 mg Bromphenol blue Adjust volume to 10 ml with ddH_2O
Unbuffered TRIS Solution (10 mM) for SRB staining	1.2 g TRIS in 1l ddH_2O Adjust pH to 10

2.1.3. Consumables

Table 2.3: List of consumables

Consumable	Manufacturer	Type	Serial number
Cell culture plate	Greiner bio-one	96-well, flat bottom	655180
Cell culture plate	Greiner bio-one	96-well, V bottom	651101
Cell culture plate	CorningInc.	48-well, flat bottom	3548
Cell culture plate	Greiner bio-one	24-well, flat bottom	662160
Cell culture plate	Corning Inc.	6-well, flat bottom	353046
Cell Star Tubes	Greiner bio-one	50 ml	227261
Cell Star Tubes	Greiner bio-one	15 ml	188271
Eppendorf tube	SARSTEDT AG	0.5 ml, white	72.699
Eppendorf tube	Carl Roth GmbH + Co.KG	1.5 ml, white	4182.1
Eppendorf tube	Carl Roth GmbH + Co.KG	1.5 ml, blue	4190.1
Eppendorf tube	Carl Roth GmbH + Co.KG	1.5 ml, green	4209.1
Eppendorf tube	Carl Roth GmbH + Co.KG	1.5 ml, red	4189.1
Eppendorf tube	Carl Roth GmbH + Co.KG	1.5 ml, yellow	4204.1
Eppendorf tube	Eppendorf	2.0 ml, white	2549
Pipette Tips	Sorenson BioScience, Inc.	0.1 - 10 µl	Colorless
Pipette Tips	Sarstedt AG & Co.	2 - 200 µl	Yellow
Pipette Tips	Ratiolab GmbH	100 - 1000 µl	Blue
Single-channel Pipette	Corning Inc.	10-100 µl	158240031
Single-channel Pipette	Corning Inc.	20-200 µl	158250088
Single-channel Pipette	Corning Inc.	100-1000 µl	058261237
Single-channel Pipette	Eppendorf	0.1-2.5 µl	P35434B
Spectrophotometer	BMG Labtech GmbH	Fluostar Omega	415-1264
Water-bath	Lauder Dr. R. Wobser GmbH	Al 25	LCB 0727-11-0094
Water-bath	Lauder Dr. R. Wobser GmbH	ECO ET 20	LY 06.1

2.1.4. Equipment

Table 2.4: List of used equipment.

Equipment	Manufacturer	Type	Serial number
Agitator, magnetic stirrer	IKA-Werke GmbH	RH B2	06.050357
Agitator, magnetic stirrer	Heidolph Instruments GmbH	MR Hei-Mix L	040700340
Centrifuge	Dako Deutschland GmbH	Stat Spin	620E50000693
Centrifuge	Thermo Fisher Scientific	Megafuge 40 R	41307652
Centrifuge	Scientific Industries Inc.	SI DD 58	DD58-1001
Centrifuge (Mirco)	Labnet International	BN 08060235	C1301B
Centrifuge (Mirco)	HERAEUS Med GmbH	Fresco 17	41250019
Electrophoresispower supplies	Bio-Rad Laboratories GmbH	Power Pac 200	285BR05538
Freezer -20°C	BSH	IQ500	GS51NYW41 (01)
Freezer -20°C	Liebherr	Med Line	LGex3410-21K 001
Freezer -80 °C	Thermo Fisher Scientific	905	827860-2521
Freezer -86 °C	Revco	ULT1386-9-V17	R10G-333095-RG
Fridge +4 °C	Liebherr	Comfort	3523-21L
Fridge +4 °C	Cool Compact Kühlgeräte G	HKMT 040-01	CC00412514
Ice maker	Scotsmen	AF 80	DD 8837 11 X
Incubator	Thermo Fisher Scientific	Heratherm OMS 60	41296334
Incubator	Binder GmbH	9040-0078	11-22649
Incubator	Binder GmbH	9040-0081	11-22190
Laboratory pump (Bench)	Carl Roth GmbH + Co.KG	Cyclo 2	1109-065
Microscope	PeqlabBiotechnologie GmbH	EVOS-fl	91-AF-4301
Mixer	Corning Inc.	Vortex Mixer	804995
Mixer	Labinco BV	LD-76	76000
Multichannel Pipette	Corning Inc.	5-50 µl	151620022
Multichannel Pipette	Corning Inc.	20-200 µl	551630277
Multichannel Pipette	Thermo Electron Co.	0.5-10 µl	CH98998 4510
Multichannel Pipette	Corning Inc.	50-300 µl	151640033

pH meter	Mettler-Toledo GmbH	Five Easy FE 20	1232315296
Pipette controller	Integra GmbH	Pipetboyacu	629619
Pipette controller	Heathrow Scientific LLC	Rota-Filler 3000	HSA05119
Refrigerator	Cool Compact Kühlgeräte G	HKMT 040-01	CC 00412516
Refrigerator	Cool Compact Kühlgeräte G	HKMN 062-01	CC 00412513
Safety workbench	Thermo Fisher Scientific	Maxisave S20201.8	41293949
Safety workbench	Thermo Fisher Scientific	Maxisave S20201.8	41293948
Scale	Kern &Sohn GmbH	ABJ 120-4M	WB 1140084
Shaker, laboratory	LTF Labortechnik GmbH	DRS 12	11DE243
Shaker, laboratory	PeqlabBiotechnologie GmbH	ES-20	010111-1107-0119
Shaker, laboratory	LTF Labortechnik GmbH	DRS 12	11DE090
Shaker, Laboratory	Corning Inc.	LSE Vortex Mixer	1101260
Single-channel Pipette	Corning Inc.	0.5-10 µl	158220060
Single-channel Pipette	Corning Inc.	2-20 µl	158230441
Single-channel Pipette	Corning Inc.	10-100 µl	158240031
Single-channel Pipette	Corning Inc.	20-200 µl	158250088
Single-channel Pipette	Corning Inc.	100-1000 µl	058261237
Single-channel Pipette	Eppendorf	0.1-2.5 µl	P35434B
Spectrophotometer	BMG Labtech GmbH	Fluostar Omega	415-1264
Water-bath	Lauder Dr. R. Wobser GmbH	Al 25	LCB 0727-11-0094
Water-bath	Lauder Dr. R. Wobser GmbH	ECO ET 20	LY 06.1
ZwickiLine	Zwick GmbH & Co. KG	2.5TN	059003

2.2 Methods

2.2.1. Preparation of gelatin (GEL) scaffolds

In this study, we used the GEL scaffold because it comprises organic (gelatin) and inorganic phases (hydroxyapatite), realistically mimicking the *in vivo* bone microenvironment (Weng *et al.*, 2020). The scaffolds were prepared according to a method recently published (Figure 2.1) (Ruoss *et al.*, 2020). Briefly, a water-based solution comprising 4.8% gelation, 10% hydroxyapatite was combined with 1% glutaraldehyde and chilled on ice. After fully mixing, the solutions were poured into

casting molds (3 mm radius, 4 cm height) and incubated for overnight at −17 °C (Figure 2.1.A). The following day, the formed matrix was stored at −80°C for 2 hours, which was used to facilitate manual slicing. Afterwards, the deep-frozen matrix was sliced into equal size (3 mm radius, 3 mm height) with the aid of a sharp blade (Figure 2.1.B). Before cell culture, GEL scaffolds were sterilized with 70% ethanol, then washed with phosphate buffered saline (PBS) and incubated with cell culture medium for stabilization and sterile control.

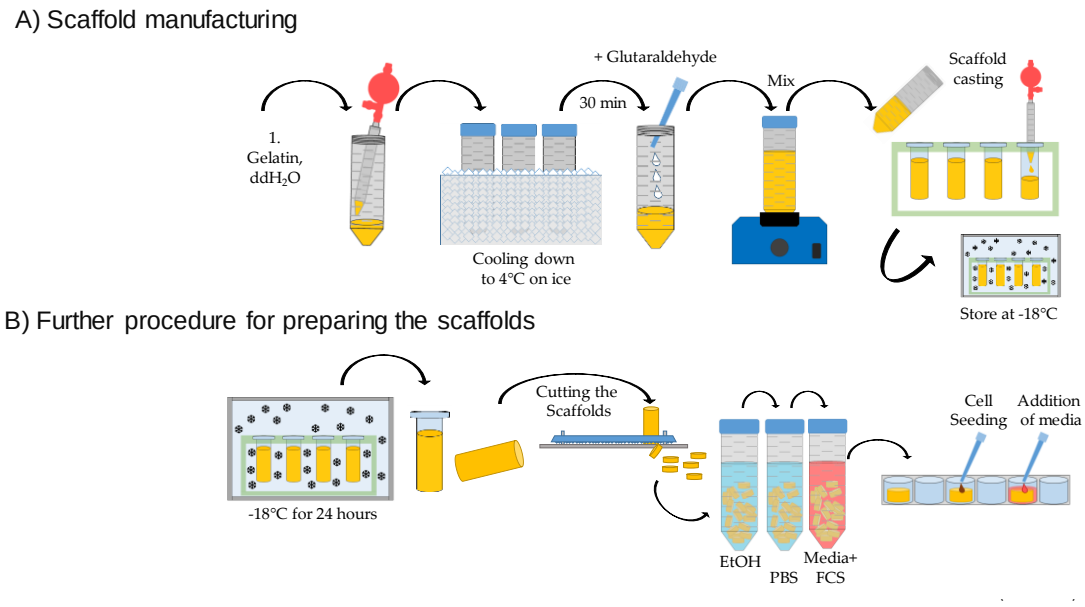

Figure 2.1 Preparation of the gelatin scaffolds. The procedure includes two steps: (A) scaffold manufacturing and (B) cutting the scaffolds and sterilization of the scaffolds before cell seeding. **(**Reproduced with permission from (Ruoss *et al.*, 2020).

2.2.2. Pore structure of GEL scaffolds

Sulforhodamine B (SRB) was used to stain organic ingredients of scaffolds and to observe the pore structure of GEL scaffolds, as described in Weng *et al.* 2020. In short, scaffolds were incubated with 0.1% SRB in the dark room for half an hour. Excessive SRB in the scaffolds was washed off using 1% acetic acid before observation and record with a microscope. ImageJ software and “BoneJ” plugins were utilized to analyze the pore structure.

2.2.3. Porosity of GEL scaffolds

The porosity was calculated based on the wet-dry weight method, as reported (Weng *et al.*, 2020). In short, scaffolds were immersed in the PBS and incubated for 60 minutes to obtain the wet weight of scaffolds. After being dried overnight in a glass desiccator, the scaffolds were weighted again to obtain the dry weight of scaffolds. The porosity of GEL scaffolds was calculated:

$$\text{porosity [\%]} = \frac{(\text{scaffold wet weight [g]} - \text{scaffold dry weight [g]})}{\text{scaffold wet weight [g]}} * 100$$

2.2.4. Stiffness of GEL scaffolds

The stiffness of GEL scaffolds was measured using Young's modulus as recently published (Weng *et al.*, 2020). A ZwickiLine Z 2.5TN machine vertically squeezed the surface scaffolds with the speed of 0.08 mm per seconds. A force sensor recorded the applied force in real time. The stiffness of GEL scaffolds was calculated:

$$\text{Young's modulus [MPa]} = \frac{applied\ force\ [N] * initial\ scaffold\ height\ [mm]}{area\ of\ the\ scaffold\ [\text{mm}^2] * change\ in\ height\ [mm]}$$

2.2.5. Cell line

Immortalized human mesenchymal stem cells (SCP-1 cell line) and human monocytic cell line THP-1 were considered as osteoprogenitor cells (Bocker *et al.*, 2008) and osteoclast precursor cells (Häussling *et al.*, 2021), respectively. SCP-1 cells were cultured in the Minimum Essential Medium Eagle alpha (MEM α) supplemented with 5% v/v fetal bovine serum (FBS). THP-1 cells were cultured in the RPMI1640 medium with 5% FBS (growing medium). All cells were maintained in a CO_2 incubator. The medium was changed twice a week.

2.2.6. 2D cell culture

SCP-1 cells and THP-1 cells were cultured in monoculture or co-culture in the 96-well plates, as recently published (Weng *et al.*, 2021). For SCP-1 monoculture, cells were plated at 3×10^3 cells/100 µL per well in osteogenic differentiation medium

(components shown in 2.1.2). For THP-1 monoculture, cells were plated at 2.4×10^4 THP-1 cells/ per well adding 100 µL of RPMI1640 medium containing 200 nM phorbol 12-myristate 13-acetate (PMA) to adhere overnight. The following day, SCP-1 cells were plated at 3×10^3 cells/ per well in the same well in 50 µL of fresh osteogenic differentiation medium and 50 µL of conditioned medium from differentiated SCP-1 cells.

For generation of bone co-culture, a THP-1 cell suspension (2.4×10^4 cells/ 100 µL per well) was plated in RPMI1640 medium containing 200 nM PMA. The following day, the growing medium was removed and washed with PBS before seeding. SCP-1 cells (3×10^3 cells/100 µL per well) were plated into the same well in the osteogenic differentiation medium (components shown in 2.1.2). In mono- and co-culture, medium was changed twice a week.

2.2.7. 3D cell culture

SCP-1 cells and THP-1 cells were cultured in monoculture or co-culture on GEL scaffolds, as recently published (Weng *et al.*, 2020). For SCP-1 monoculture, 1×10^4 cells/15 µL per scaffold were dripped on the top of GEL scaffolds. After 4 hours of incubation at 37°C, 500µL of osteogenic differentiation medium (components shown in 2.1.2) was gently added. For THP-1 monoculture, 8×10^4 cells/15 µL per scaffold were seeded into the top of GEL scaffolds. After 4 hours, 500 µL of bone growing medium supplemented 200 nM PMA to induce THP-1 cells into adherent macrophages. The following day, the growing medium was changed by 250 µL of fresh osteogenic differentiation medium and 250 µL of conditioned medium from differentiated SCP-1 cells.

For generation of bone co-culture, a THP-1 cell suspension (8×10^4 cells/ 15 µL per scaffold) was seeded on the top of GEL scaffolds. After 4 hours of incubation at 37°C, 500 µL of the growing medium with 200 nM PMA was gently added. The following day, the growing medium was removed and washed with PBS before seeding. SCP-1 cells (1×10^4 cells/15 µL per scaffold) were seeded into the same scaffold. After 4 hours, 500 µL of the osteogenic differentiation medium was gently added. In mono-

and co-culture, medium was changed twice a week.

2.2.8. Preparation of cigarette smoke extract (CSE)

CSE was prepared based on the previously reported method (Sreekumar *et al.*, 2018). Commercial cigarettes (Marlboro Red Label) used in this study were bought in cigarettes shops. In short, one cigarette was constantly burned with the aid of a pump. The smoke was delivered into the 25 ml of 50:50 mix of MEM α: RPMI plain medium in a typical gas bottle. The absorbance of CSE was measured at 320 nm by an Omega Plate Reader and an absorbance of 0.7 was regarded as 100% CSE. CSE was sterile filtered before experimentation and the filtered solution was further adjusted to different concentrations (1%, 5%, and 10%) with osteogenic differentiation medium.

2.2.9. Resazurin Conversion Assay

For detection of mitochondrial activity in bone cells cultured on the GEL scaffolds, cells were gently washed with PBS before 500 µL of 0.0025% w/v resazurin working solution was added. Following incubation for 2 h, the fluorescence intensity of formed resorufin was evaluated by an Omega Plate Reader (Weng *et al.*, 2020).

2.2.10. Live staining with Calcein AM-Hoechst

For visualization of viable cells and nuclei, cells were incubated in a staining dye (components shown in 2.1.2, 100 µL for 2D and 500 µL for 3D) for 20 min. After washing off excessive dye solution with PBS, stained cells were observed and captured with the aid of a fluorescence microscope (Aspera-Werz *et al.*, 2020, Häussling *et al.*, 2021).

2.2.11. Sulforhodamine B (SRB) Staining

For detection of total protein content in bone cells in 96-well plates, cells were fixed 100% ethanol overnight at -20°C. Following washing off excessive ethanol with PBS, fixed cells were stained with a dye (components shown in 2.1.2) for 30 min. Excessive SRB was washed off by 1% acetic acid. After adding 1% acetic acid to dissolve SRB

bounded to cells, the absorbance intensity was determined by an Omega Plate Reader (Aspera-Werz *et al.*, 2020).

2.2.12. DNA quantification

For detection of total DNA content in bone cells cultured on the GEL scaffolds, cells were wadded 250 µL of 50 mM 98°C NaOH for 5 min. Afterwards, these scaffolds were stored at −20°C overnight to improve DNA yield. The following day, frozen samples were thawed at 60°C for 15 min before adding 250 µL of a 100 mM Tris buffer. The impurities from these DNA samples were removed by centrifugation at 2000× g for 10 min. For total DNA quantitative analysis, 2 µL of DNA samples were dripped on the LVIS Micro Drop Plate and measured by the Omega Plate Reader (Weng *et al.*, 2020).

2.2.13. Carbonic anhydrase II (CA II) activity

For detection of early stage of osteoclast differentiation in bone cells cultured on the GEL scaffolds or 96-well plates, cells were gently washed with PBS before adding CAII standard assay (components shown in 2.1.2, 100 µL for 2D and 500 µL for 3D) for 15 min. The absorbance intensity was determined using a Omega Plate Reader (Weng *et al.*, 2021, Häussling *et al.*, 2021).

2.2.14. Tartrate-resistant acid phosphatase (TRAP) activity assay

For detection of osteoclast function in bone cells cultured on the GEL scaffolds or 96-well plates, the cell culture supernatant (30 µL for 2D and 30 µL for 3D) was combined with 90 µL of TRAP standard assay (components shown in 2.1.2) into a fresh 96-well plate and cultured for 6 hours at 37°C. To stop the reaction, 90 µL of 1 M NaOH was added into the well. The absorbance was determined using a Omega Plate Reader (Weng *et al.*, 2021, Häussling *et al.*, 2021).

2.2.15. Alkaline phosphatase (AP) activity

For detection of osteoblast function in bone cells cultured on the 96-well plates, cells

were gently washed with PBS once before adding 100 µL of AP standard assay (components shown in 2.1.2). After incubation for 30 min at 37°C, absorbance intensity was measured using a Omega Plate Reader (Weng *et al.*, 2021).

2.2.16. Immunofluorescence staining

Cells were fixed as shown above (Section 2.2.11). Fixed cells were permeabilized with 0.2% v/v Triton-X-100 for 15 min and then blocked with BSA blocking buffer (components shown in 2.1.2) for 1 h to band unspecific sites. Cells were stained by TRITC-phalloidin (1:2000) and Hoechst 33342 (1:1000) for 2 h. After washing twice with PBS, cells were visualized by fluorescence microscopy. For counting the number of SCP-1 as well as THP-1 cells in co-culture, total number of cells were counted, followed by the number of THP-1 cells based on the morphology of the osteoclast-like cells. Multinuclear cells (more than two nucleus) with actin-ring formation were regarded as the osteoclast-like cells. The number of osteoclast-like cells were subtracted from total number of cells to achieve the number of osteoblast-like cells.

2.2.17. Dot Blot analysis

To assess changes in bone resorption and formation markers secreted by bone-resorbing and bone-forming cells, fifty microliters of supernatants were transferred to membrane using a vacuum-assisted dot blot. Ponceau S staining was used for visualization of protein dots. After extensive washing with TBS-T, the membrane was blocked with BSA blocking buffer (components shown in 2.1.2) for 2 h to band unspecific sites and then incubated with primary antibody overnight (Table 2.5). After extensive washing with TBS-T, the membrane was incubated with secondary antibodies for 2 h. The signal was visualized by a CCD camera and measured with ImageJ software (Weng *et al.*, 2021).

Table 2.5. The antibodies used in this study.

Antibody	Catalog No.	Company	Dilution
RANKL	500-M46	Peprotech, Hamburg, GER	1:1000
OPG	500-P149	Peprotech, Hamburg, GER	1:1000
PINP	abx131414	Abbexa, Aachen, GER	1:1000
OCN	sc-365797	Santa Cruz, Heidelberg, GER	1:1000
Goat anti-mouse IgM	sc -2064	Santa Cruz, Heidelberg, GER	1:10,000
Goat anti-rabbit IgG	sc -2020	Santa Cruz, Heidelberg, GER	1:10,000

RANKL = receptor activator of nuclear factor kappa-B ligand; OPG = osteoprotegerin; PINP = procollagen type I N-terminal propeptide; OCN = Osteocalcin.

2.2.18. Zymography

To evaluate changes in matrix degradation marker (MMP-9) secreted by bone-resorbing cells, five microliters of supernatants were combined with fifteen microliters of loading buffer (components shown in 2.1.2) and transferred to zymography gels. After electrophoresis at 120 V, the zymography gels first washed three times with 2.5% Triton X-100 and further washed five times with ddH_2O. Following incubation with zymography developing buffer (components shown in 2.1.2) for 24 hours at 37°C, the gels were dyed with Coomasie blue. The signals were detected with ImageJ software (Ehnert *et al.*, 2011).

2.2.19. Statistics

Data were represented as bar diagrams. At least three independent experiments were performed, each at least in triplicate. Comparisons were executed using 1-way or 2-way ANOVA when one or more independent variables were compared between groups. GraphPad Prism software was used for analysis. **The statistical methods of this thesis were discussed with Johann Jacoby from the Institute of Clinical Epidemiology and Applied Biometry at the University of Tübingen**.

3. Results

3.1. Physical characterization of the GEL scaffold

The pore area of GEL scaffolds was visualized by SRB staining (12,615 ± 620 μm^2; Figure 3.1.A). GEL scaffolds possessed appropriate stiffness (25 ± 1.3 KPa; Figure 3.1.B). The porosity of the GEL scaffolds was determined *via* their wet and dry weight (Figure 3.1.C). GEL scaffolds exhibited excellent porosity (85 ± 0.3%), comparable to that of Osbone® (80%), a commercial bone graft material (Bernhardt *et al.*, 2011).

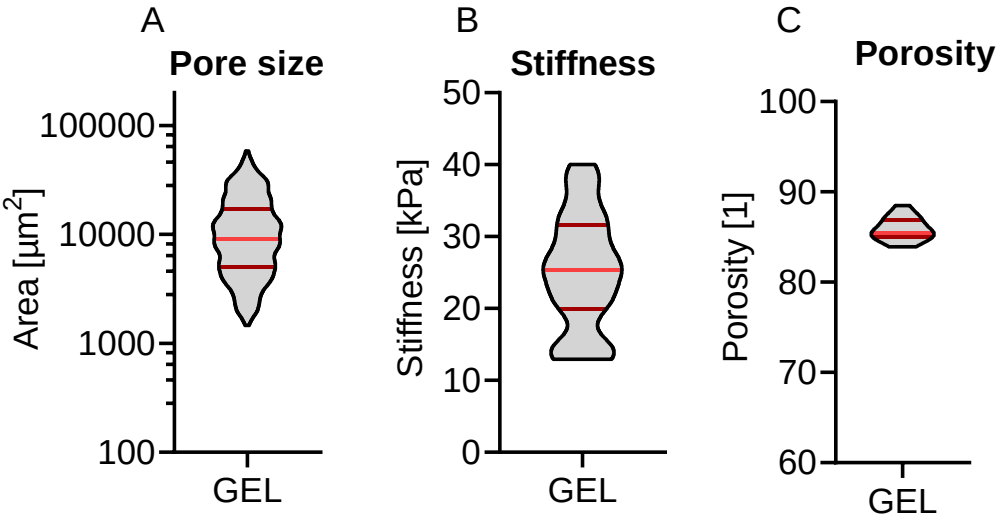

Figure 3.1 Physical characterization of the GEL scaffold. (A) Pore area and (B) stiffness were analyzed by ImageJ. (C) Scaffold porosity expressed as %. Data are shown as violin plots showing median and quartiles (N = 3, n ≥ 4).

3.2. Analysis of average area of bone cells

To determine whether SCP-1 and THP-1 cells are capable of migrating inside of scaffolds, we calculated the average circularity area of these two types of cells from the bone co-culture system and then compared them with the pore area of the GEL scaffolds. We found that the mean area was 253.1 ± 8.9 μm^2 for SCP-1 cells (Figure 3.2.A and B) and 182 ± 6.4 μm^2 for THP-1 cells (Figure 3.2.A and C). The area was remarkably small in SCP-1 and THP-1 cells compared with the pore area of the GEL scaffolds. Therefore, these bone cells are capable of migrating inside of GEL scaffolds.

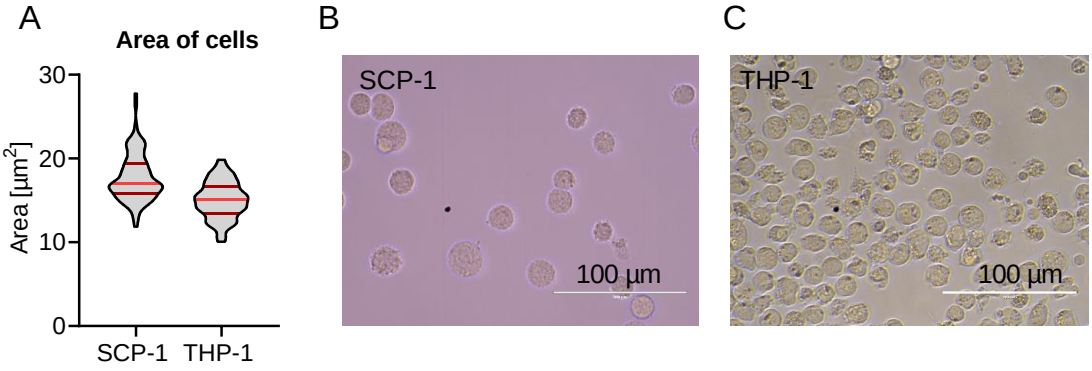

Figure 3.2 Average area of SCP-1 and THP-1 cells. (A) The areas of these two types of bone cells were analyzed by ImageJ. Data are expressed as violin plots showing median and quartiles (N = 3, n ≥ 20). Representative microscopic pictures of (B) SCP-1 and (C) THP-1 cells used to calculate circularity area.

3.3. Assessment of appropriate co-culture medium mixtures for SCP-1 and THP-1 cells

SCP-1 and THP-1 monocultures in 96-well plates were treated by mixing different proportions of MEM α and RPMI (75%:25%; 50%:50%; 25%:75%) to develop an appropriate co-culture medium for sustaining the survival and differentiation of both cell types.

3.3.1. SCP-1 cells

For SCP-1 cells, cells cultivated with100% MEM α was utilized as a control group. Measurement of SRB staining exhibited a remarkable decrease of total protein content in cells treated with 25% MEM α or 0% MEM α at both time points (days 7 and 14; Figure 3.3.1.A), compared to the control group. The osteoblast function (AP activity) was not greatly altered in SCP-1 cells treated with 75% MEM α or 50% MEM α on days 7 and 14 (Figure 3.3.1.B), compared to the control group. Microscope images of actin staining confirmed the previous findings (Figure 3.3.1.C): SCP-1 cells, stretched cells with a mononuclear phenotype, were rarely observed in 0% MEM α after 14 days.

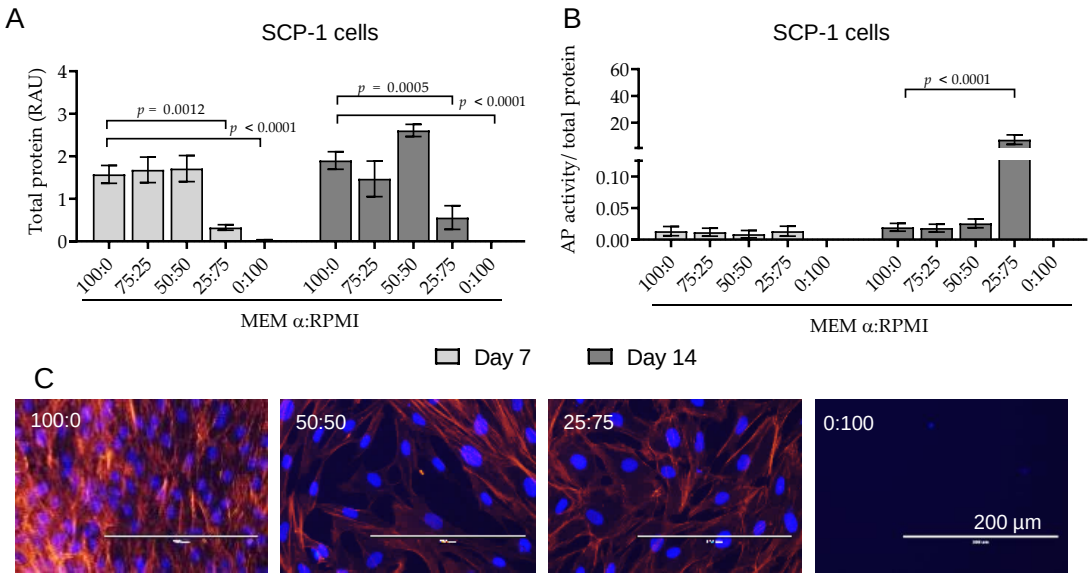

Figure 3.3.1 Analysis of the effects of mixing different proportions of MEM α and RPMI on SCP-1 cell survival and differentiation. SCP-1 cells (N = 3, n = 4) were treated by mixing different proportions of MEM α and RPMI. (A) Total protein content and (B) AP activity/total protein content were determined in SCP-1 cells after 7 and 14 days. (C) Representative images of actin staining with Phalloidin-TRITC (in red) and Hoechst 33342 (in blue) was used to visualize stretched cells with a mononuclear phenotype (SCP-1 cells) after 14 days. Data were represented as bar diagrams. Statistical analysis: 2-way ANOVA test.

3.3.2. THP-1 cells

For THP-1 cells, cells cultivated with 100% RPMI was utilized as a control group. Cells exposed to 25% RPMI or 0% RPMI had a significantly lower total protein content at both time points (days 7 and 14; Figure 3.3.2.A), compared to the control group. The osteoclast function (CAII activity) was not largely affected in THP-1 cells treated with 75% RPMI α or 50% RPMI on days 7 and 14 (Figure 3.3.2.B), compared to the control group. Microscope images of actin staining illustrated that the number of multinuclear cells with acting ring structure representing THP-1 cells derived osteoclast, was dramatically declined in the absence of RPMI after 14 days (Figure 3.3.2.C).

Taken together, these results showed that the medium containing 50% MEM α and 50% RPMI sustained SCP-1 and THP-1 cell survival and differentiation; therefore, this medium ratio was identified being appropriate for our bone co-culture system.

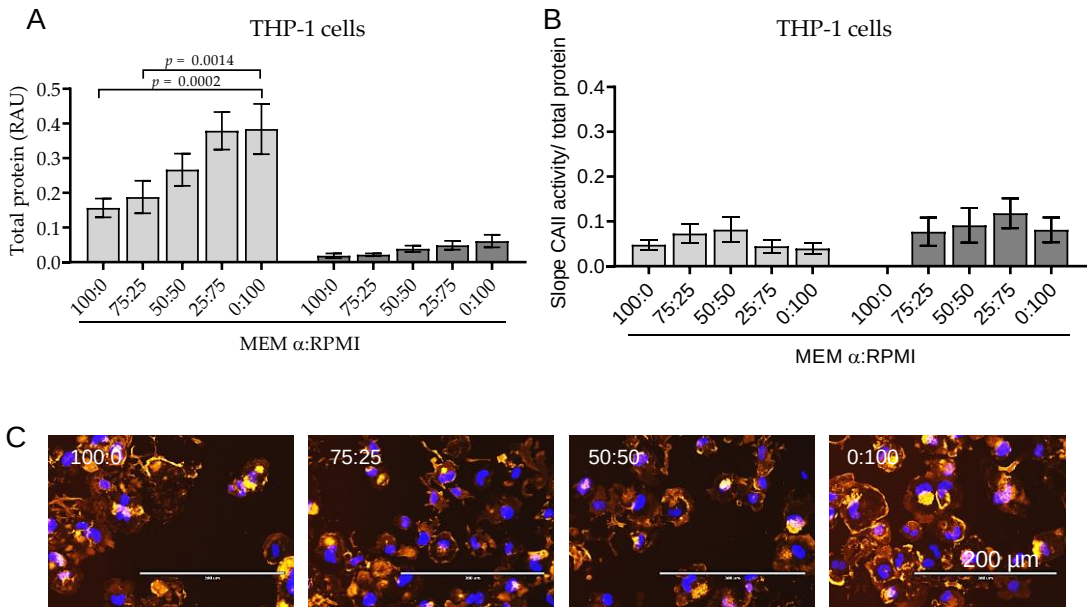

Figure 3.3.2 Analysis of the effects of mixing different proportions of MEM α and RPMI on THP-1 cell survival and differentiation. THP-1 cells (N = 3, n = 4) were treated by mixing different proportions of MEM α and RPMI. (A) Total protein content and (B) CAII activity/total protein content were determined in the THP-1 cells after 7 and 14 days. (C) Representative images of actin staining with Phalloidin-TRITC (in red) and Hoechst 33342 (in blue) was used to visualize roundish cells with a multinucleated phenotype and actin rings (THP-1 cells) after 14 days. Data were represented as bar diagrams. Statistical analysis: 2-way ANOVA test.

3.4. Analysis of SCP-1 and THP-1 cell attachment on the scaffolds

SCP-1 and THP-1 cells were seeded as monocultures onto the scaffolds. On days 1, 4, 7, and 14, cell attachment was analyzed using mitochondrial activity and Calcein AM–Hoechst staining. Our results demonstrated that there was a positive correlation between DNA content and mitochondrial activity with the cultivation time of SCP-1 cell on the scaffolds (Figure 3.4.A and B). THP-1 cells had a slow increase in total DNA content and mitochondrial activity when cultured on the scaffolds over the time (Figure 3.4.A and B). Microscopic assessment of live staining displayed viable SCP-1 and THP-1 cells on the GEL scaffolds (Figure 3.4.C), indicating appropriate SCP-1 and THP-1 attachment onto GEL scaffolds.

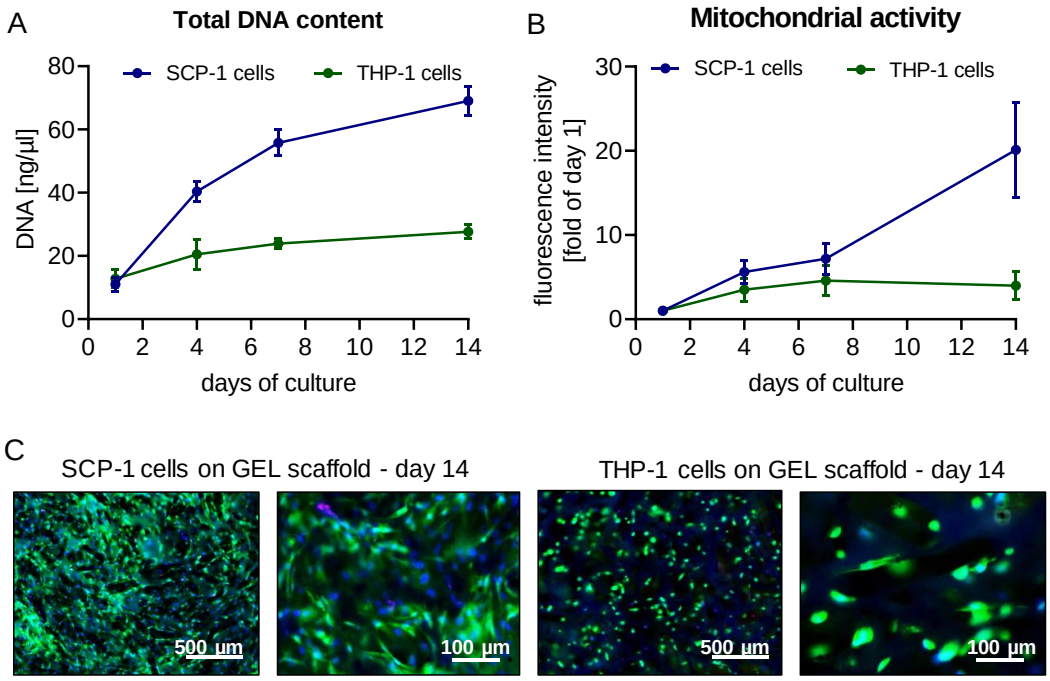

Figure 3.4 Analysis of SCP-1 and THP-1 cell attachment onto the GEL scaffolds. SCP-1 and THP-1 cells (N = 3, n = 3) were seeded onto the GEL scaffolds. (A) Total DNA content and (B) mitochondrial activity were determined in SCP-1 and THP-1 monocultures by day 1, 4, 7, and 14. (C) Representative images of live staining with Calcein AM (in green) and Hoechst 33342 (in blue) was used to visualize SCP-1 and THP-1 cells after 14 days. Data are represented as the mean ± SEM.

3.5. Evaluation of appropriate co-culture proportions of SCP-1 and THP-1 cells

To find a suitable proportion of SCP-1 and THP-1 cells that represent the function of bone forming and resorbing cells in our system, two cell proportions (1:4 and 1:8) were evaluated. SCP-1 and THP-1 monocultures were used as the control group. The SCP-1 monoculture displayed an increase in total protein content over time. On days 7 and 14, no protein was detectable in the THP-1 monoculture (4) and expression was very low in the THP-1 monoculture (8). The co-culture with 1:8 seeding ratio of SCP-1: THP-1 cells had a lower total protein content than the 1:4 co-culture after 14 days ($p > 0.05$; Figure 3.5.A). The count of SCP-1 cells was remarkably higher in the cell model with a cell proportion of 1:4, while the count of THP-1 cells was remarkably lower in the cell model with a cell proportion of 1:8. No THP-1 cells were detectable in the 1:4 co-culture, indicating that this co-culture model could not sustain the morphology (Figure

3.5.B and C). The osteoblast function was not affected with the number of osteoblast seeded in the scaffolds (Figure 3.5.D).

TRAP and CAII activity were used to represent osteoclast function (Figure 3.5.E and F). The variation of osteoclast function was smaller and more stable in the co-cultures than in THP-1 monoculture (Figure 3.5.E and F). CAII activity was almost doubled in the 1:8 co-culture compared to the 1:4 co-culture by 14 days (Figure 3.5.E). Therefore, the 1:8 co-culture was chose for further experiments, due to that better maintained the number of functional THP-1 cells.

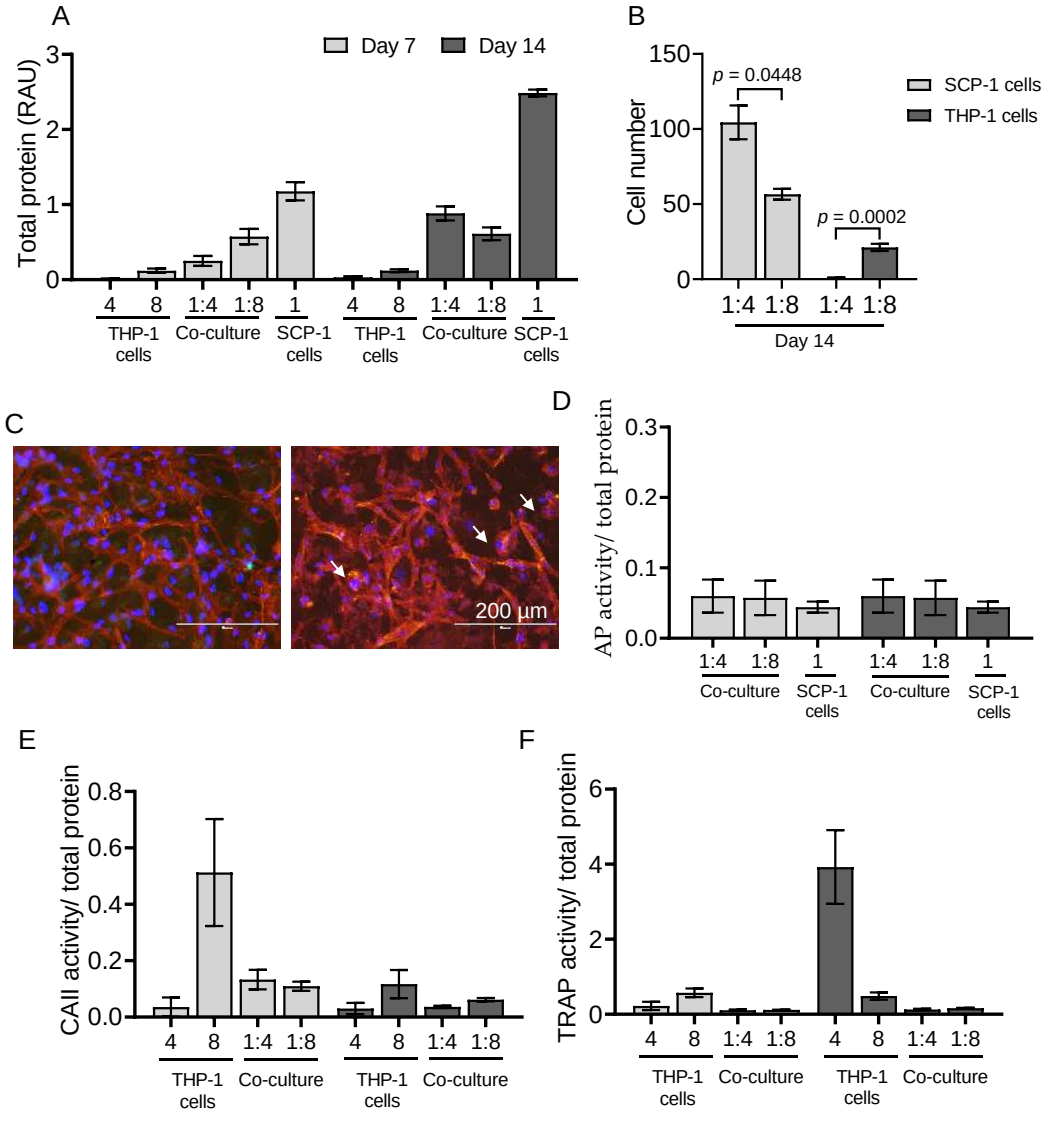

Figure 3.5 Evaluation of appropriate co-culture proportions of SCP-1 and THP-1 cells. SCP-1 and THP-1 cells (N = 3, n = 3) were cultured alone (monoculture) or together (co-culture) at two seeding proportions (1:4 & 1:8). (A) Total protein content was determined in SCP-1 and THP-1 monocultures and co-cultures at different time

points (7 and 14 days). (B) The count of SCP-1 and THP-1 cells in the co-cultures was calculated after 14 days. (C) Representative images show stretched cells with a mononuclear phenotype (SCP-1 cells) and roundish cells with a multinucleated phenotype and actin rings (THP-1 cells, represented in white arrows) by 14 days. Osteoblast function: (D) AP activity was evaluated in SCP-1 monocultures and co-cultures with THP-1 cells at two proportions after 14 days. (E) CAII and (F) TRAP actives were evaluated in THP-1 monocultures and co-cultures with SCP-1 cells at two proportions after 14 days. Data were represented as bar diagrams. Statistical analysis: 2-way ANOVA test.

3.6. Assessment of the effects of CSE on viability in SCP-1 and THP-1 monocultures and co-culture systems

SCP-1 and THP-1 monocultures and co-culture systems were exposed to various concentrations of CSE (1%, 5%, and 10%) for 14 days. As shown in Figure 3.6, the mitochondrial activity of the SCP-1 monoculture and co-culture systems increased over time. The mitochondrial activity of the THP-1 monoculture was elevated from day 3 to day 7, then reduced from day 7 to day 14. The CSE exposure remarkably suppressed mitochondrial activity in SCP-1 and THP-1 monocultures and co-culture systems in a dose- and time-dependent manner (Figure 3.6.A–C). On day 3, the mitochondrial activity was not greatly altered in any of conditions tested when compared to untreated cells for all culture models evaluated (Figure 3.6.A). On day 7, the mitochondrial activity was remarkably decreased in THP-1 monoculture ($p < 0.05$; Figure 3.6.A), SCP-1/THP-1 co-culture ($p < 0.01$; Figure 3.6.B), and SCP-1 monoculture ($p < 0.001$; Figure 3.6.C) following exposure to 10% CSE compared with untreated cells. On day 14, all tested cell culture models exhibited a significant decrease in mitochondrial activity following exposure to 5% or 10% CSE compared with untreated cells. Exposure to 10% CSE decreased mitochondrial activity in the co-culture system by more than 50% after 7 days ($p < 0.05$; Figure 3.6.B) and 14 days ($p < 0.01$; Figure 3.6.B) compared to untreated cells, indicating that 10% CSE strongly affected bone cell viability. In view of these results, 5% CSE was chosen to be used in the subsequent experiments.

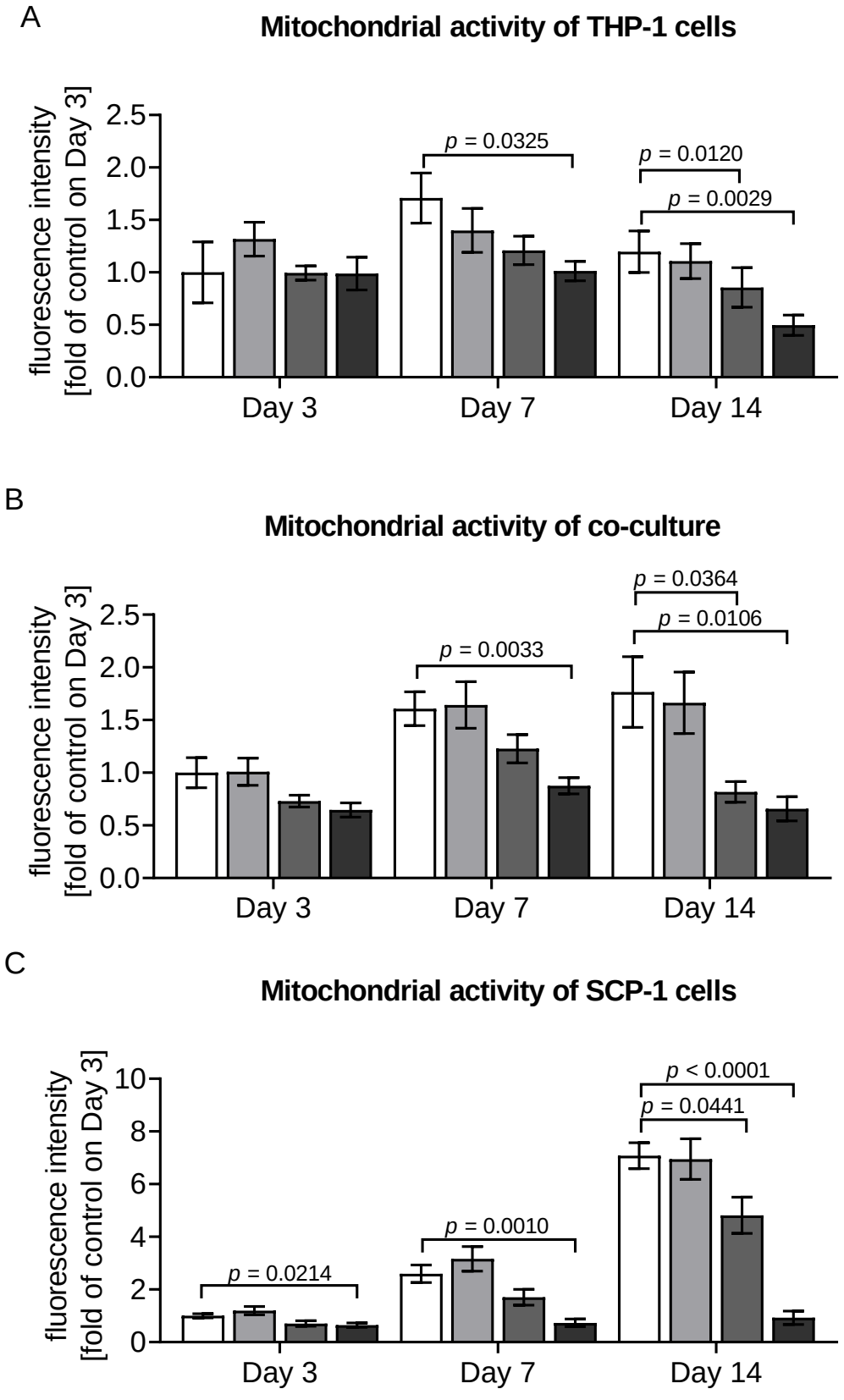

Figure 3.6 Assessment of the effects of CSE on viability in SCP-1 and THP-1 monocultures and co-culture systems. SCP-1 and THP-1 cells (N = 3, n = 3) cultured alone (monoculture) or together (co-culture) were exposed to increasing concentrations

of CSE (1%, 5%, and 10%) for 3, 7, and 14 days. Mitochondrial activity was determined in (A) THP-1 monoculture, (B) co-culture, and (C) SCP-1 monoculture after 3, 7, and 14 days. Data were represented as bar diagrams. Statistical analysis: 2-way ANOVA test.

3.7. Evaluation of the effects of magnesium chloride supplementation on viability in SCP-1 and THP-1 monocultures and co-culture systems

3.7.1. Acute exposure

In order to screen the nontoxic concentration of magnesium chloride supplementation for bone cells, SCP-1 and THP-1 monocultures and co-culture systems were supplemented with various concentrations of magnesium chloride (0.1, 1, 10, and 100 mM) for 24 h. We found that all tested models acutely exposed to 100 mM magnesium chloride revealed a remarkable reduction in total DNA content, compared to untreated cells. Acute exposure to 10 mM magnesium chloride decreased the total DNA content in the THP-1 monoculture ($p > 0.05$; Figure 3.7.1.A), SCP-1 monoculture ($p < 0.05$; Figure 3.7.1.B), and co-culture ($p > 0.05$; Figure 3.7.1.C). These results indicate that the nontoxic concentration of magnesium chloride supplementation for SCP-1 and THP-1 cells is below 10 mM.

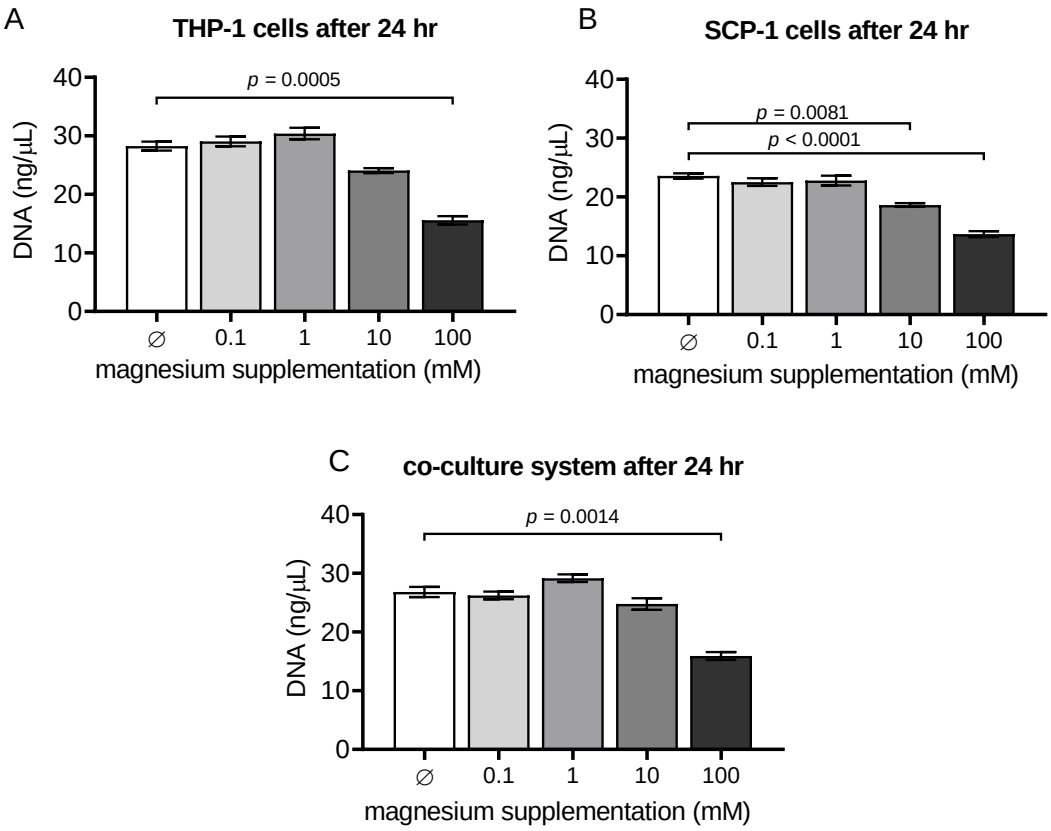

Figure 3.7.1 Evaluation of the acute effects of magnesium chloride supplementation on viability in SCP-1 and THP-1 monocultures and co-culture systems. SCP-1 and THP-1 cells (N = 3, n = 3) cultured alone (monoculture) or together (co-culture) were acutely exposed to increasing concentrations of magnesium chloride for 24 h. The total DNA content was determined in (A) SCP-1 monoculture, (B) THP-1 monoculture, and (C) co-culture. Data were represented as bar diagrams. Statistical analysis: one-way ANOVA test.

3.7.2. Chronic exposure

In order to assess the long-term effects of magnesium chloride supplementation on the viability of SCP-1 and THP-1 cells, cultures were chronically exposed to increasing concentrations of magnesium chloride (1, 2, 4, 6, and 8 mM) for 14 days. The total DNA content decreased in the THP-1 monoculture in a dose-dependent manner (Figure 3.7.2.A). In the SCP-1 monoculture, the total DNA content remained unchanged in cells supplemented with increasing concentrations of magnesium chloride (Figure 3.7.2.B). In the co-culture system, the total DNA content decreased significantly in cells exposed to 6 mM ($p < 0.001$; Figure 3.7.2.C) or 8 mM magnesium chloride ($p < 0.0001$; Figure 3.7.2.C) compared with untreated cells. Based on these

results, we can conclude that the nontoxic concentration of magnesium chloride supplementation for SCP-1 and THP-1 cells is up to 4 mM.

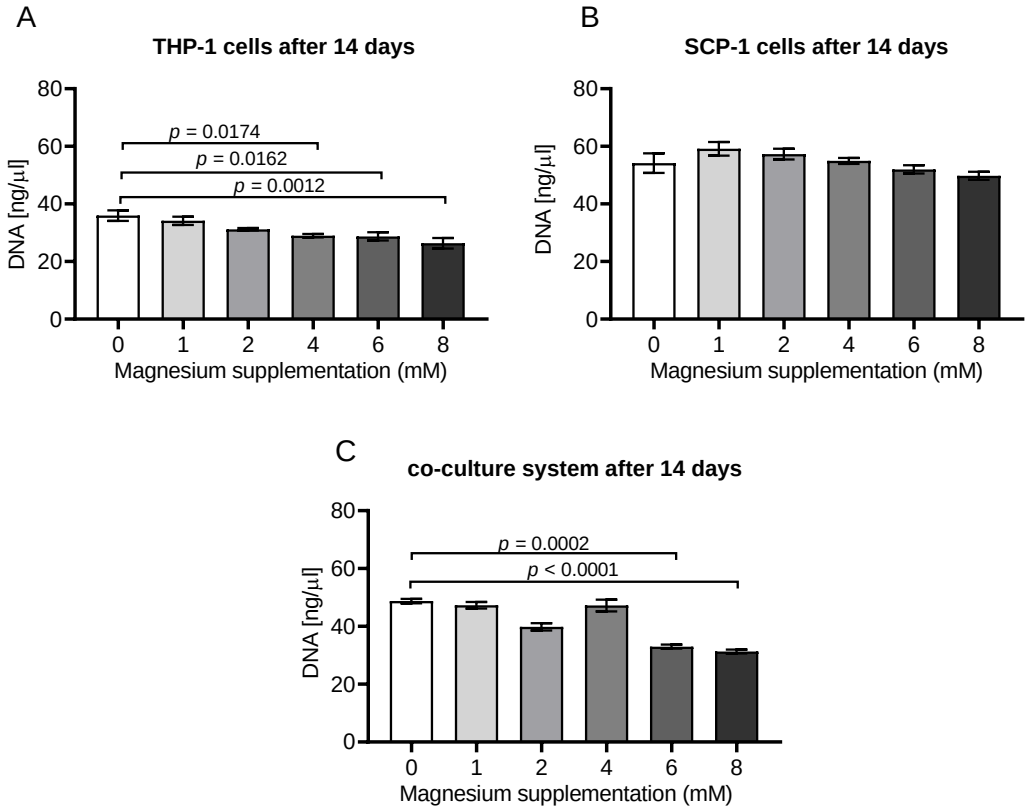

Figure 3.7.2 Analysis of the long-term effects of magnesium chloride supplementation on viability in SCP-1 and THP-1 monocultures and co-culture systems. SCP-1 and THP-1 cells (N = 3, n = 3) cultured alone (monoculture) or together (co-culture) were chronically exposed to increasing concentrations of magnesium chloride for 14 days. The total DNA content was determined in (A) SCP-1 monoculture, (B) THP-1 monoculture, and (C) co-culture. Data were represented as bar diagrams. Statistical analysis: one-way ANOVA test.

3.8. Evaluation of the impact of magnesium chloride supplementation on viability and functionality in 3D co-culture systems impaired by CSE

Magnesium chloride supplementation is known to exert an essential role in bone metabolism and has been shown to prevent bone resorption and promote bone formation (Li *et al.*, 2019). To evaluate whether magnesium chloride supplementation could reverse the deleterious effects of CSE in 3D bone co-culture systems, bone cells

were treated with 5% CSE in combination with 1 or 4 mM magnesium chloride supplementation.

3.8.1. Viability

Bone cells exposed to 5% CSE displayed a remarkable decrease in mitochondrial activity ($p < 0.001$; Figure 3.8.1.A) and total DNA content ($p < 0.0001$; Figure 3.8.1.B) on day 14 compared with untreated cells. Mitochondrial activity was comparable in the co-cultures exposed to 5% CSE alone and the co-culture exposed to 5% CSE in combination with 4 mM magnesium chloride supplementation (Figure 3.8.1.A). Additional supplementation of the 3D bone co-cultures with 4 mM magnesium chloride for 14 days increased the mitochondrial activity by 24% ($p > 0.05$; Figure 3.8.1.A) and the total DNA content by 31% ($p < 0.001$; Figure 3.8.1.B).

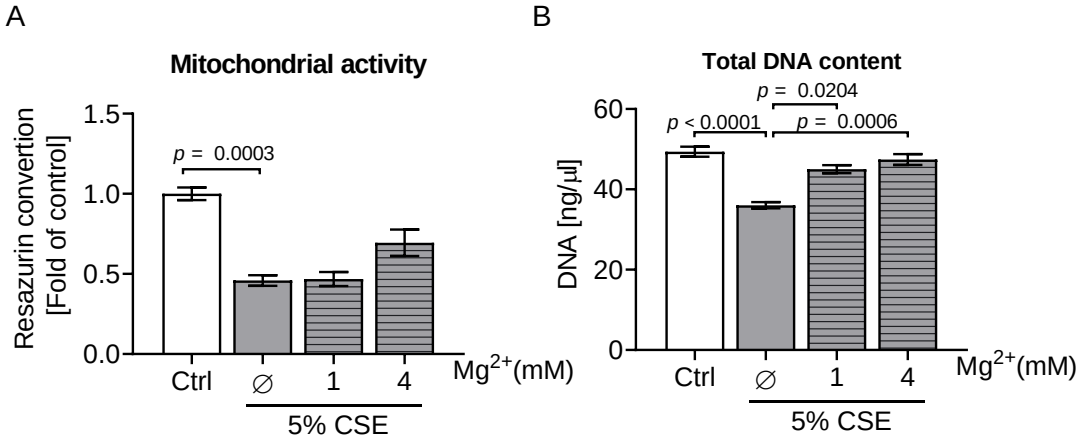

Figure 3.8.1 Analysis of the influence of magnesium chloride supplementation on viability in 3D bone co-cultures impaired by CSE. SCP-1 and THP-1 cells (N = 3, n = 3) cultured together (co-culture) on the GEL scaffolds were treated with 5% CSE in combination with 1 or 4 mM magnesium chloride supplementation. (A) Mitochondrial activity and (B) total DNA content were assessed in the co-cultures after 14 days. Data were represented as bar diagrams. Statistical analysis: one-way ANOVA test.

3.8.2. Functionality

Co-cultures exposed to 5% CSE presented a remarkable elevation in TRAP activity ($p < 0.01$; Figure 3.8.2.A) and CAII activity ($p < 0.05$; Figure 3.8.2.B) on day 14

compared with untreated cells. Supplementation with magnesium chloride at either 1 or 4 mM reduced TRAP activity in bone cells exposed to 5% CSE ($p > 0.05$ for 1 or 4 mM magnesium chloride supplementation; Figure 3.8.2.A). Additional supplementation with 4 mM magnesium chloride for 14 days remarkably reduced CAII activity ($p < 0.01$; Figure 3.8.2.B) in the 3D bone co-cultures exposed to 5% CSE.

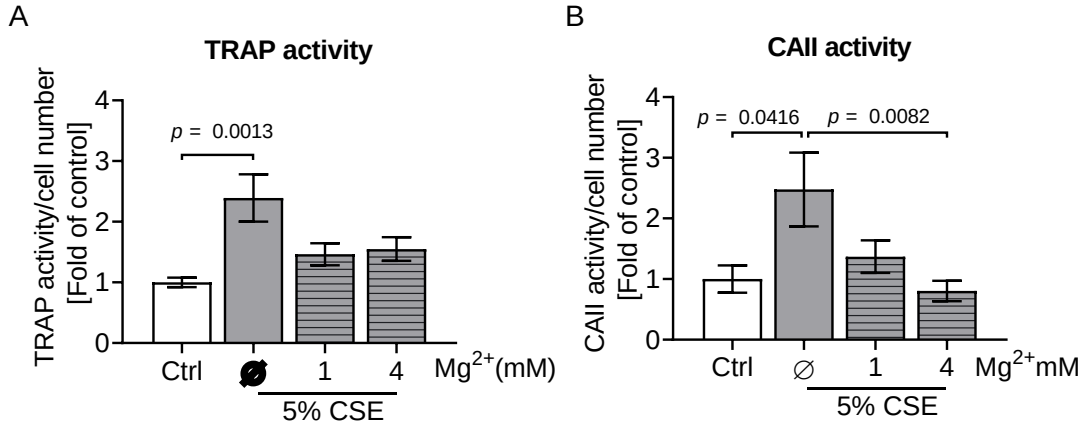

Figure 3.8.2 Analysis of the influence of magnesium chloride supplementation on functionality in 3D bone co-cultures impaired by CSE. SCP-1 and THP-1 cells (N = 3, n = 3) cultured together (co-culture) on the GEL scaffolds were treated with 5% CSE in combination with 1 or 4 mM magnesium chloride. (A) TRAP activity and (B) CAII activity were assessed in the co-cultures after 14 days. Data were represented as bar diagrams. Statistical analysis: one-way ANOVA test.

3.9. Evaluation of the impact of magnesium chloride supplementation on matrix formation and resorption in 3D co-culture systems impaired by CSE

To evaluate the changes in matrix formation and resorption in bone cells exposed to 5% CSE in combination with magnesium chloride supplementation, the supernatants of co-cultures were measured for three matrix remodeling markers: procollagen type I N-terminal propeptide (PINP), a collagen formation marker (Weng *et al.*, 2021); MMP-9, an extracellular matrix degradation marker (Duellman *et al.*, 2012); and osteocalcin (OCN), a late osteogenic marker (Häussling *et al.*, 2021). We found that bone cells exposed to 5% CSE showed a remarkable reduction in PINP levels ($p < 0.0001$; Figure 3.9.A) and OCN levels ($p < 0.0001$; Figure 3.9.B) and elevation in MMP-9 activity ($p > 0.05$; Figure 3.9.C). This implies that exposure to CSE can facilitate the

formation of an osteoporotic environment in the 3D bone co-culture system. The presence of 4 mM magnesium chloride remarkably increased PINP levels ($p < 0.05$; Figure 3.9.A) and OCN levels ($p < 0.05$; Figure 3.9.B) and reduced MMP-9 activity ($p < 0.05$; Figure 3.9.C) in bone cells exposed to 5% CSE.

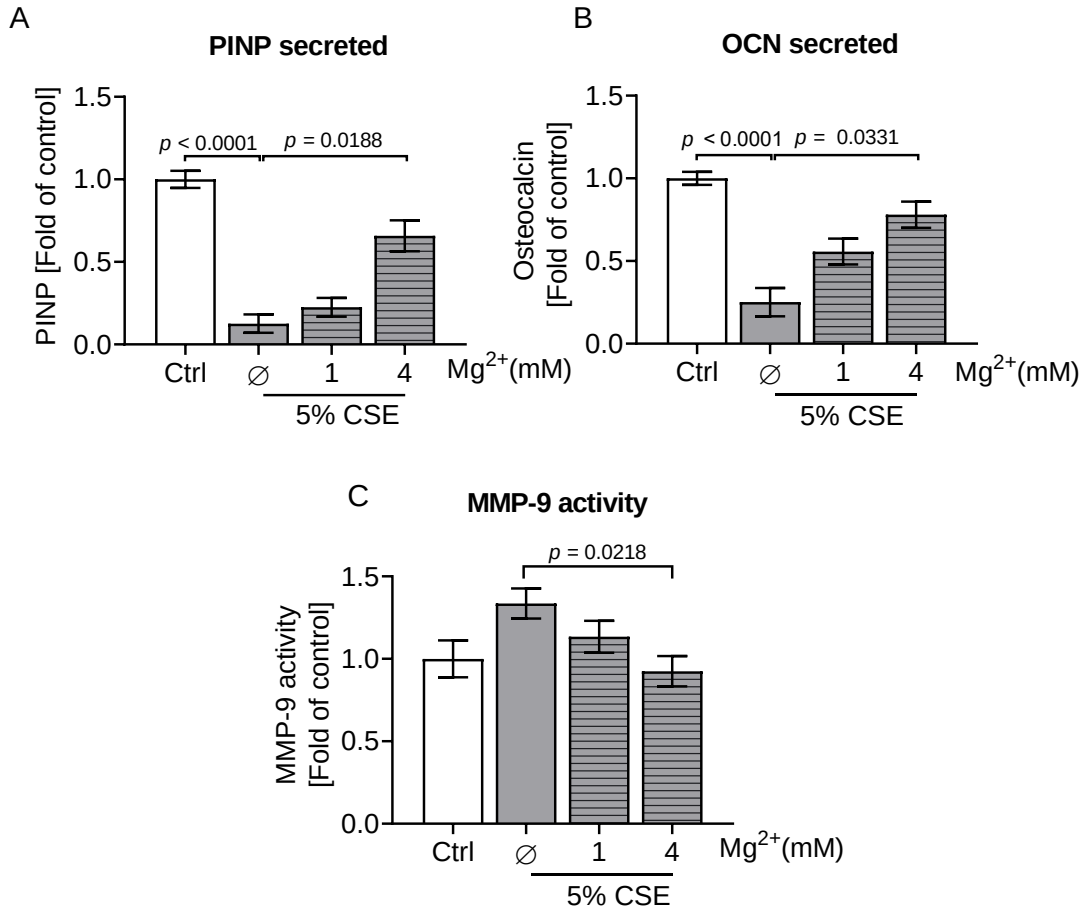

Figure 3.9 Analysis of the influence of magnesium chloride supplementation on matrix formation and resorption in 3D bone co-cultures impaired by CSE. SCP-1 and THP-1 cells (N = 3, n = 3) cultured together (co-culture) on the GEL scaffolds were treated with 5% CSE in combination with 1 or 4 mM magnesium chloride supplementation. (A) PINP levels, (B) OCN levels, and (C) MMP-9 activity were evaluated in the supernatants of co-cultures after 14 days. Data were represented as bar diagrams. Statistical analysis: one-way ANOVA test.

3.10. Evaluation of the impact of magnesium chloride supplementation on RANKL/OPG balance in 3D co-culture systems impaired by CSE

RANKL is a crucial bone turnover marker required for inducing osteoclast differentiation (Weng *et al.*, 2021, Udagawa *et al.*, 2021). We found that RANKL levels

were comparable in bone cells exposed to 5% CSE and untreated cells after 14 days ($p > 0.05$; Figure 3.10.A). At the same time, levels of its antagonist OPG were markedly decreased in the 3D bone co-culture system treated with 5% CSE compared to untreated cells ($p < 0.01$; Figure 3.10.B). The RANKL/OPG ratio was remarkably higher in bone cells after exposure to 5% CSE than in the untreated control ($p < 0.05$; Figure 3.10.C). Additional supplementation with 4 mM magnesium chloride for 14 days remarkably reduced the RANKL/OPG ratio ($p < 0.0001$; Figure 3.10.C) in the 3D bone co-cultures exposed to 5% CSE. The anti-osteoclastic effect of magnesium chloride supplementation was more pronounced at 4 mM than at 1 mM.

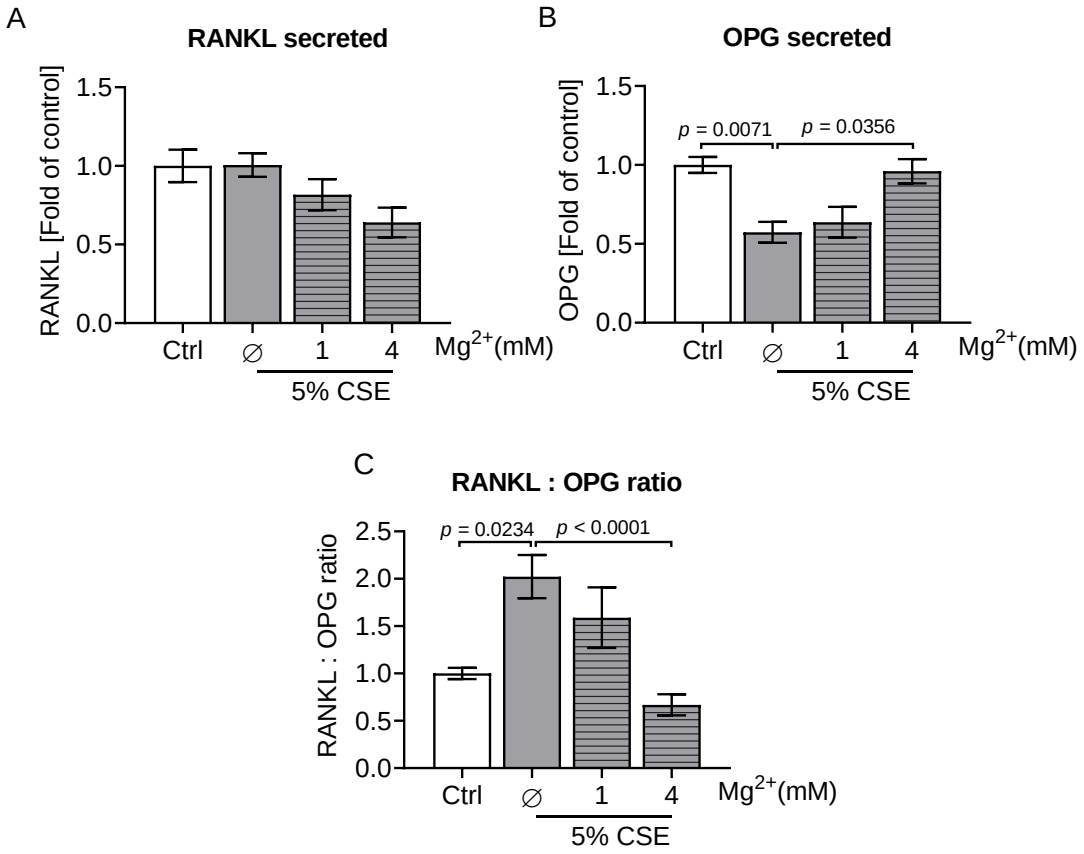

Figure 3.10 Analysis of the influence of magnesium chloride supplementation on RANKL/OPG balance in 3D bone co-cultures impaired by CSE. SCP-1 and THP-1 cells (N = 3, n = 3) cultured together (co-culture) on the GEL scaffolds were treated with 5% CSE in combination with 1 or 4 mM magnesium chloride supplementation. (A) RANKL levels, (B) OPG levels, and (C) RANKL:OPG ratio were evaluated in the supernatants of co-cultures after 14 days. Data were represented as bar diagrams. Statistical analysis: one-way ANOVA test.

Chapter 4

4. Discussion

Delayed or nonunion fracture healing is one of the medical complications following severe injuries or surgical intervention (Lynch *et al.*, 2008, Mills *et al.*, 2017). Currently, surgical revisions are required to treat these postoperative complications, resulting in extended hospitalization and increased medical costs (Schlickewei *et al.*, 2019, Cheng and Shoback, 2019).

It is well known that long-term exposure to CS contributes to a high risk of delayed or nonunion fracture healing (Sloan *et al.*, 2010, Moghaddam *et al.*, 2010). During the period of bone fracture healing, CS has the potential to interfere with bone metabolism through suppressing the osteogenic differentiation of osteoblast precursor cells and promoting the osteoclastic differentiation of osteoclast precursor cells, contributing to an osteoporotic bone environment in bone cells (Yoon *et al.*, 2012, Ko *et al.*, 2015). However, the mechanism by which CS induces an osteoporotic bone environment is not yet fully understood. Understanding the regulatory mechanism(s) in bone cells impaired by CS will enable us to obtain insights into the development of CS-induced osteoporotic bones and screen relevant preventive treatment strategies for smokers with osteoporotic bones. Hence, this research seeks to construct a reliable and effective *in vitro* model of bone cells exposed to CSE that simulates the osteoporotic changes observed in smokers, which may facilitate understanding of the potential mechanisms and may identify new therapeutic approaches for smokers with 'osteoporotic' bones.

Currently, no standard *in vitro* models exist to simulate the processes of fracture healing, involving the osteogenesis and osteoclastogenesis of precursor cells (Ehnert *et al.*, 2020). Most of the bone *in vitro* studies were performed in 2D co-culture models, however, 2D bone co-culture models do not possess a strong capacity to represent the microenvironment, geometry chemistry, and interactions of the bone cells observed *in vivo* (Ehnert *et al.*, 2020). Several studies have revealed that 3D cell cultures enhance bone cell survival, proliferation, and differentiation, since cells are subjected to physiological conditions analogous to those in the body (Thein-Han and Misra, 2009,

Di Maggio *et al.*, 2011). In view of this, 3D bone culture systems exhibit several improvements for osteogenic differentiation of osteoblast-like cells and osteoclastic differentiation of osteoclast-like cells, compared to 2D culture systems (Häussling *et al.*, 2021). In the present study, we developed a valid and reliable 3D bone co-culture system including osteogenesis and osteoclastogenesis cultured on a GEL-based cryogel, realistically mimicking the *in vivo* bone microenvironment. The first step in developing such a model was to develop the bone-like material (GEL-based cryogel) and characterize its physical properties (Weng *et al.*, 2020). We observed a GEL scaffold stiffness of 25 ± 1.3 kPa (Weng *et al.*, 2020). It has been reported that scaffolds with stiffness of 11–40 kPa enhance the osteogenic differentiation of osteoblast-like cells (Engler *et al.*, 2006, Huebsch *et al.*, 2010). In addition, the porosity of the GEL scaffold (85%) was comparable with that of the synthetic hydroxyapatite bone graft substitute used in dental surgery (Osbone® Curasan with 80% porosity that resembles human cancellous bone) (Bernhardt *et al.*, 2011). Based on these results, we concluded that the GEL scaffold possessed a high degree of interconnectivity and optimal stiffness, and formed an appropriate 3D platform for the survival and differentiation of bone cells *in vitro* (Weng *et al.*, 2020).

Next, we proceeded to optimize the medium and the seeding ratio between SCP-1 and THP-1 cells to maintain their viability and functionality. For the medium optimization, both cell types were vulnerable to variations in the composition of the culture medium, particularly when over half of the original medium was replaced with the medium applied to cultivate the other cell type. Since the viability and functionality of SCP-1 and THP-1 cells were maintained within a 50:50 mix of RPMI and MEM α medium, this appropriate medium was used in the later experiments. To optimize the seeding ratio, we initially seeded a higher number of THP-1 cells than SCP-1 cells, since the osteoclastic differentiation from THP-1 cells into multinucleated osteoclastic cells is achieved by cell fusion (Jansen *et al.*, 2012). We found that a co-culture system with a 1:4 seeding ratio (SCP-1/THP-1) displayed only osteoblast-like cells; osteoclast-like cells were barely detectable by 14 days. Interestingly, the system with a 1:8 seeding ratio differentiated into approximately 70% osteoblasts and 30% osteoclasts by day 14

and better represented the proportion of bone forming/resorbing observed in bone tissue (Florencio-Silva *et al.*, 2015). Moreover, the co-culture system with a 1:8 seeding ratio had higher osteoclast function than that with a 1:4 seeding ratio by 14 days. Therefore, the co-culture system with a cell ratio of 1:8 (SCP-1/THP-1) cultured on the GEL scaffold maintained the viability and functionality of bone cells.

It is known that CS exhibits highly adverse effects on 2D bone culture systems (Aspera-Werz *et al.*, 2018, Aspera-Werz *et al.*, 2020, Zhu *et al.*, 2020). However, the effects of CS on 3D bone culture systems have remained elusive. In this study, the 3D bone cell culture system was exposed to three different concentrations of CSE. We observed that chronic exposure to 1% CSE for 14 days was not able to cause negative consequences in 3D SCP-1 or THP-1 monocultures or the 3D co-culture system, whereas the negative effects of 10% CSE on this 3D bone culture systems viability were lethal. Interestingly, 5% CSE negatively affected the mitochondrial activity of 3D SCP-1 and THP-1 monocultures, and the 3D co-culture system. Additionally, 5% CSE was capable of suppressing osteoblast differentiation of SCP-1 cells (PINP and OCN levels) and inducing osteoclast differentiation of THP-1 cells (TRAP and CAII activity) in the 3D bone co-culture system, which eventually contributed to a reduction in bone mineral content of the GEL scaffold. These results are in agreement with recent research indicating that CS is associated with osteoporotic-like changes in bone cells (Ko *et al.*, 2015, Zhu *et al.*, 2020). Therefore, 5% CSE was used for the further experiments, since it induces osteoporotic-like changes in our 3D bone co-culture system, as observed in smokers with osteoporotic bones. Additionally, 5% CSE is associated with smoking about 10 cigarettes per day (Aspera-Werz *et al.*, 2019).

Mg, an essential cofactor, is involved in various biological activities regulating energy metabolism, DNA transcription, and protein synthesis (Vernon, 1988, Paolisso *et al.*, 1990, Mieczkowski *et al.*, 2013). Moreover, Mg, a crucial component of human bone mineral, is widely applicable in orthopedic applications due to its ability to promote osteogenesis and inhibit osteoclastogenesis (Wu *et al.*, 2017, Zhao *et al.*, 2017). In line of these findings, it is not surprising, that Mg deficiency is thought to be one cause of delayed or nonunion fracture healing (Rude and Olerich, 1996, Rude *et al.*, 1999).

Furthermore, based on clinical observations, Mg deficiency is positively related to damaged bone microstructure and bone loss (Freudenheim *et al.*, 1986, Tranquilli *et al.*, 1994, Tucker *et al.*, 1999). Another study revealed that insufficient Mg intake also resulted in reduced bone mass by enhancing bone resorption and suppressing bone formation in an animal model (Rude *et al.*, 2003).

Interestingly, several clinical studies have reported that heavy smokers have a remarkably lower serum Mg concentration compared to nonsmokers (Khand *et al.*, 2015, Ata *et al.*, 2015). Based on these findings, we hypothesized that Mg deficiency may be one of the potential reasons why long-term exposure to smoke elevates the risk of impaired bone fracture healing. Subsequently, we assumed that Mg supplementation may be a reliable and valid strategy for smokers with Mg deficiency and osteoporotic-like bones. In this study, we observed that the nontoxic concentration of Mg supplementation for the 3D SCP-1/THP-1 co-culture system was up to 4 mM. It is worth noting that the physiological concentration of Mg is 1 mM (Zocchi *et al.*, 2021). Subsequently, we compared the influence of two Mg supplementation concentrations (1 and 4 mM) on bone cells exposed to 5% CSE.

Our results revealed that additional supplementation with 4 mM Mg for 14 days significantly increased the total DNA content and mitochondrial activity in the 3D bone co-culture system exposed to CSE. This protective effect of Mg supplementation was more pronounced at 4 mM than at 1 mM. Additionally, co-incubation of the CSE-exposed 3D bone co-culture with 4 mM Mg reduced TRAP and CAII activity when compared to those exposed to CSE alone. These results are in agreement with previous research which showed the anti-osteoclastic effects of Mg supplementation on osteoclastic differentiation and bone resorption (Wu *et al.*, 2014, Wang *et al.*, 2018, Miao *et al.*, 2019, Mammoli *et al.*, 2019). Wang *et al.* (Wang *et al.*, 2018) reported that Mg supplementation inhibited osteoclastic differentiation of RAW264.7 cells induced by lipopolysaccharide and Mammoli *et al.* (Mammoli *et al.*, 2019) revealed that Mg supplementation suppressed osteoclastic differentiation of U937 cells.

In addition to its anti-osteoclastic capacity, Mg is also capable of facilitating the mineralization of bone-forming cells (Zhang *et al.*, 2019, Hung *et al.*, 2019, Kong *et*

al., 2019, Qi *et al.*, 2021). Matrix mineralization occurs in the late phases of osteogenic differentiation, in which several osteogenic factors are involved (Aspera-Werz *et al.*, 2018, Sreekumar *et al.*, 2018). For instance, PINP, a collagen formation marker, is synthesized by osteoblasts (Salam *et al.*, 2018). OCN, synthesized by osteoblasts, is engaged in binding hydroxyapatite to the bone matrix (Ducy *et al.*, 1996, Wei and Karsenty, 2015). In this work, supplementation with 4 mM Mg obviously elevated matrix deposition in CSE-induced cells by upregulating PINP and OCN levels. Apart from matrix deposition of bone-forming cells, matrix remodeling is also regulated by matrix degradation of bone-resorbing cells (Hadjidakis and Androulakis, 2006, Alford *et al.*, 2015). MMP-9 is a proteolytic enzyme which has been related to matrix degradation (Delaisse *et al.*, 2003, He *et al.*, 2013). We observed that co-incubation of the CSE-exposed 3D bone co-culture with 4 mM Mg reduced matrix degradation (MMP-9 activity) when compared to that exposed to CSE alone. Based on these results, we concluded that 4 mM Mg supplementation is able to reverse the CSE-induced impaired matrix mineralization by upregulating matrix formation and downregulating matrix degradation.

It has been reported that the interaction between RANKL and RANK stimulates osteoclastogenesis. RANKL, a membrane protein, is synthesized and released by osteoblast-like cells. This protein is capable of binding to RANK receptor located on osteoclast-like cells, activating osteoclastogenesis (Wada *et al.*, 2006). As a decoy receptor for RANKL, OPG suppresses osteoclastogenesis by binding to RANKL (Udagawa *et al.*, 2021). Therefore, the balance between RANKL and OPG exerts a vital role in regulating bone metabolism (Boyce and Xing, 2008). In our model, consistent with an elevated RANKL:OPG ratio, osteoclast differentiation markers (CAII and TRAP activity) also increased in the presence of CSE. Supplementation with 4 mM Mg effectively inhibited osteoclast activity in CSE-induced bone cells by switching to upregulation of OPG. These results are in accord with previous studies indicating that Mg has a potential capacity to reduce bone resorption by reducing the RANKL:OPG ratio (Rude *et al.*, 2005, Bae and Kim, 2010, Sahin *et al.*, 2021).

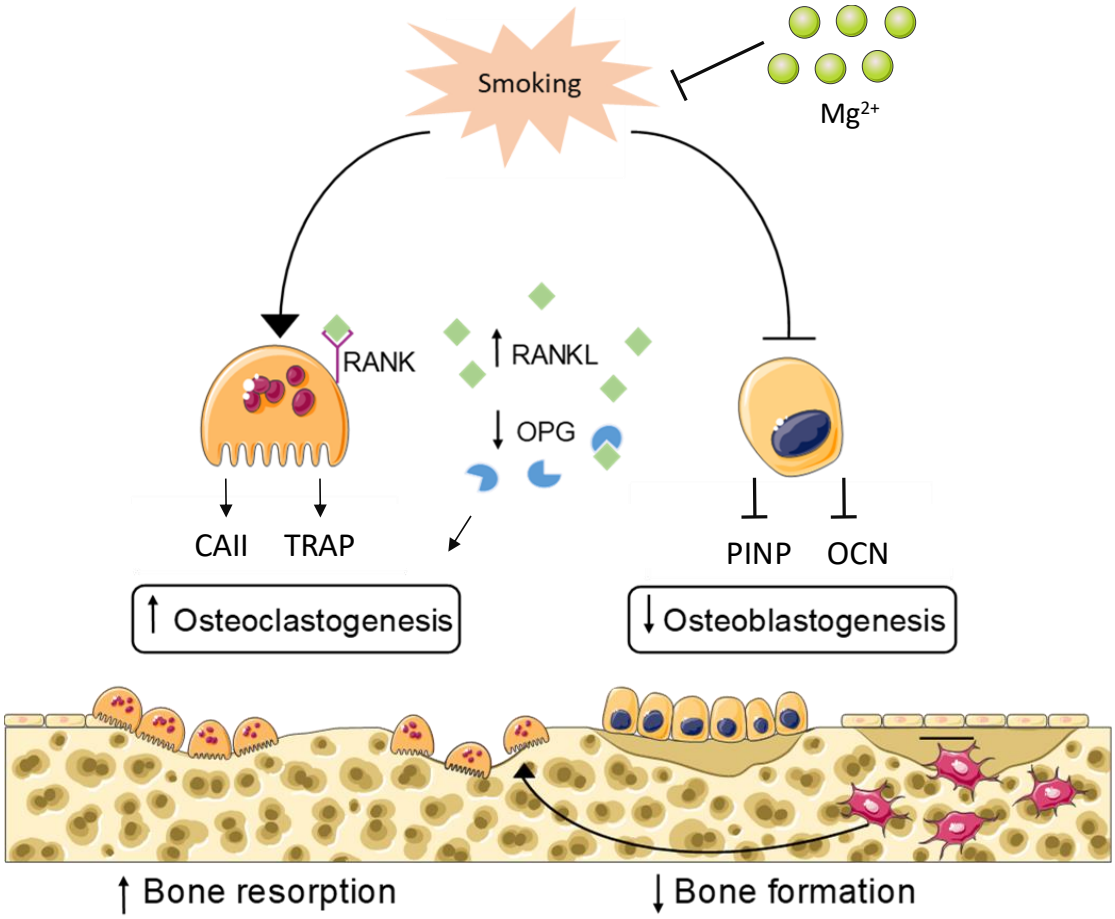

4.1 Schematic diagram representing the protective effects of Mg supplementation on the 3D bone co-cultures impaired by CSE. Supplementation with Mg obviously elevated matrix deposition in CSE-induced cells by upregulating PINP and OCN levels. Supplementation with Mg effectively inhibited osteoclastogenesis in CSE-induced bone cells by switching to upregulation of OPG. The image was generated with the assistance of Servier Medical Art (https://smart.servier.com/).

Wnt/β-catenin canonical signaling pathway may be one potential mechanism, which is involved in the regulation of RANKL/OPG balance. According to reports, Wnt/β-catenin canonical pathway in osteoblast/pre-osteoblast can reduce RANKL/OPG ratio, inhibiting osteoclast differentiation and bone resorption. (Glass *et al.*, 2005, Spencer *et al.*, 2006). In addition to suppressing osteoclastogenesis, it also enhances osteogenic differentiation of MSCs (Imamura *et al.*, 2020, Thomas and Jaganathan, 2022), bone formation (Zhang *et al.*, 2020, Carrillo-López *et al.*, 2021), and mineralization (Yang *et al.*, 2018, Ruan *et al.*, 2021) by elevating the expression of osteogenic markers, like osterix, OPG, and OCN. Therefore, Wnt/β-catenin canonical pathway appears to exert

a dual role in bone metabolism, improving osteoblastogenesis on the one hand and suppressing osteoclastogenesis on the other. Understanding and characterizing the Wnt/β-catenin canonical pathway in detail is believed to be critical to guiding the interaction between osteoblast and osteoclast (Spencer *et al.*, 2006, Choi *et al.*, 2019, Wu *et al.*, 2020).

Wnt ligands, secreted glycoproteins, are engaged in multiple biological processes like cell migration (Liu *et al.*, 2021, Li *et al.*, 2022), proliferation (Wang *et al.*, 2022), differentiation (Ji and Sun, 2022). These soluble proteins are capable of activating Wnt/β-catenin canonical pathway (Liu *et al.*, 2022, Zhang *et al.*, 2022). In this pathway, β-catenin, a crucial signal molecule, exerts a vital role in the development and growth of bone-related cells, which may further influence the quality and integrity of bone tissue (Chen *et al.*, 2021, Liu *et al.*, 2021). Upregulation of β-catenin has been shown to enhance osteoblastic differentiation of osteoblast precursor cells by activating the canonical Wnt pathway (Zhang *et al.*, 2013). Downregulation of β-catenin has been reported to suppress osteoblastic bone formation of osteoblast-like cells by inhibiting the canonical Wnt pathway (Qiang *et al.*, 2008). Nevertheless, the detailed mechanism of this pathway in bone metabolism is not fully understood and being investigated (Xu *et al.*, 2013). To our knowledge, Wnt ligands (Wnt 3a & 5a) are capable of enhancing the accumulation of β-catenin in the cytoplasm of osteoblast-like cells by integrating with receptor complex including Frizzled and LRP5/6 (Liu *et al.*, 2022, Wagner *et al.*, 2022). Afterward, the accumulated β-catenin transfers into the nucleus to modulate the transcription of osteogenic-related genes, like *Osterix* and *OPG* (Cui *et al.*, 2021, Xu *et al.*, 2022). Finally, the accumulated OPG integrates with RANKL and prevents it from integrating with RANKL located on osteoclast-like cells, suppressing osteoclastogenesis (Chu *et al.*, 2021, Guo *et al.*, 2022). In this study, supplementation with Mg effectively inhibited osteoclastogenesis in CSE-induced bone cells by switching to upregulation of OPG. Although we did not explore Wnt/β-catenin signaling by which supplementation with Mg inhibited osteoclast activity in the 3D bone co-cultures impaired by CSE, oral supplementation with Mg has been shown to enhance the quality and integrity of bone tissue in an animal model by activating Wnt/β-

catenin signaling (Chu *et al.*, 2021). Similarly, nanofibers rich in Mg have been reported to stimulate MSCs' survival, proliferation, and osteogenic differentiation through activating Wnt/β-catenin signaling (Guler *et al.*, 2021). Further investigations are required to clarify whether Mg supplementation is capable of suppressing CSE-induced osteoporotic changes in 3D bone co-cultures through Wnt/β-catenin signaling.

In summary, we established an *in vitro* bone co-culture system containing osteoblast precursor cells (SCP-1 cells) and osteoblast precursor cells (THP-1 cells) co-cultured on a scaffold, mimicking the bone metabolism *in vivo* as closely as possible. Our data suggested that 5% CSE was capable of inhibiting osteoblast differentiation of SCP-1 cells and inducing osteoclast differentiation of THP-1 cells in the 3D bone co-culture system, which eventually contributed to osteoporotic-like changes in 3D bone fracture healing system. Supplementation of Mg enhanced osteoblast activity and suppressed osteoclast activity in bone cells impaired by CSE through the downregulation of RANKL:OPG ratio. The protective effects of Mg supplementation were more pronounced at 4 mM than at 1 mM.

This work has made many advances to reduce osteoporotic-like changes in bone cells related to CS. However, serval critical issues remain to be resolved with the goal of developing therapeutic interventions to prevent or treat osteoporotic bones in smokers. Several clinical studies compared serum Mg levels in heavy smokers and nonsmokers and found that heavy smokers had a remarkably lower serum Mg level compared to nonsmokers (Ata *et al.*, 2015, Khand *et al.*, 2015). Currently, the reason for the Mg deficiency in smokers is unclear. It is reported that Mg deficiency may be attributed to insufficient dietary intake (Meng *et al.*, 2021, Kebir and Zahzeh, 2022) or inadequate absorption of Mg (Barbagallo *et al.*, 2021, Fiorentini *et al.*, 2021). Despite unclear mechanisms, these findings have crucial implications for clinical practice research. Heavy smokers are more likely to have Mg deficiency and may even have osteoporotic bones. Currently, serum Mg concentration is not routinely assessed in German hospitals for heavy smokers who need orthopedic surgery. Therefore, we recommend that surgeons monitor serum Mg concentration pre- and postoperatively as routine, especially for heavy smokers. When patients are diagnosed with Mg deficiency,

surgeons may recommend Mg supplementation either orally or *via* intravenous infusion to prevent or treat osteoporotic bones caused by smoking.

We demonstrated that Mg supplementation reduced cigarette smoke–associated cell damage in the 3D bone fracture healing model, indicating Mg supplementation may be a promising strategy for smokers with osteoporotic bones to improve bone quality. Generally, Mg could be administrated as Mg chloride or Mg sulfate (Harris *et al.*, 1952). Relative to Mg chloride, Mg sulfate is more widely applied in clinical practice since it has the characteristics of long residence time (Silva Filho *et al.*, 2021, Zhang *et al.*, 2022, Soleimanpour *et al.*, 2022). However, Mg sulfate has been reported to have a higher toxic potential than Mg chloride (Durlach *et al.*, 2005). For this reason, we selected Mg chloride instead of Mg sulfate for the study.

We observed that the protective effects of Mg supplementation were more pronounced at 4 mM than at 1 mM. It means that supplementation with 4 mM Mg is a possible dose of treating CSE-induced cell damage in the 3D bone co-culture model. It is worth noting that this effective concentration of Mg in this study is above the physiological concertation. Supplementation with 4 mM Mg may contribute to negative undesired effects on other organ systems, like heart, liver, and kidney. Further clinical investigations are required to clarify the Mg administration patterns, such as dose, and duration.

Our bone co-culture model only comprised osteoblast precursor cells (SCP-1 cells) and osteoblast precursor cells (THP-1 cells), representing a part of bone metabolism *in vivo*. This is a relatively complex repair process comprising a variety of cells, like vessel forming endothelial cells (Yin *et al.*, 2021), participating immune cells (Ehnert *et al.*, 2021), chondrocytes (Wong *et al.*, 2021), bone forming and resorbing cells (Zhu *et al.*, 2021). To mimic bone fracture healing *in vivo* as closely as possible, not only extra immune cells and chondrocytes but also endothelial cells need to be considered. Therefore, this multicellular system is capable of representing bone metabolism as closely as possible to what occurs *in vivo*.

In this study, we used glutaraldehyde to crosslink gelatin (organic component) and hydroxyapatite (inorganic component). However, glutaraldehyde has been reported to

exert toxic effects on cells (Rideout *et al.*, 2005, Zeiger *et al.*, 2005). Several researchers have used a non-toxic method, UV irradiation, for crosslinking bone-like materials (Krishnakumar *et al.*, 2019, Rico-Llanos *et al.*, 2021). Using UV irradiation to crosslink organic and inorganic bone components instead of glutaraldehyde would be attractive. Additionally, the scaffold lacks crucial growth factors that exert a pivotal role in the development and growth of bone-related cells (Hynes, 2009, Bourgine *et al.*, 2014). Cell-derived extracellular matrix scaffold may be a promising alternative to possess not only physical characterization of 3D materials but also growth factors, realistically mimicking the *in vivo* bone microenvironment. Currently, we have shown that a simple method (heat treatment) allows us to construct an osteoblast-like cell-derived matrix, providing a non-toxic and stable platform for the development and growth of bone-related cells (Weng *et al.*, 2021). Thus, it would be interesting to integrate the osteoblast-like cell-derived matrix into our model. An appropriate co-culture model contains multiple cells related to bone fracture healing and ideal bone-like material, which will be beneficial for exploring in-depth the influence of CS on bone metabolism and corresponding coping strategies for smokers with osteoporotic-like bones.

Chapter 5

5. Summary

It is well established that CS has an adverse impact on bone homeostasis, contributing to increased risk of fragility fractures and impaired fracture healing. CS is capable of suppressing osteoblast function and improving osteoclast function.

Mg is engaged in promoting osteogenic differentiation of osteoblast progenitor cells and suppressing osteoclastic differentiation of osteoclast progenitor cells. Not surprisingly, Mg deficiency has been associated with bone loss. Interestingly, a clinical study reported that heavy smokers had a remarkably lower serum Mg level compared to nonsmokers. Based on this finding, we hypothesized that Mg supplementation is capable of reversing the adverse impacts of CS on bone metabolism.

In this study, we constructed an *in vitro* bone co-culture system containing SCP-1 cells and THP-1 cells co-cultured on a scaffold, mimicking the reparative phase of bone fracture healing *in vivo* as closely as possible. Then, we investigated the impact of Mg supplementation on the 3D bone co-culture system impaired by CSE. We observed that 5% CSE is capable of enhancing osteoclastic differentiation and inhibiting osteogenic differentiation in the 3D bone co-culture system, creating an osteoporotic microenvironment as observed in the smokers with osteoporotic bones. Supplementation with 4 mM Mg effectively inhibited osteoclast function (TRAP and CAII activity) and enhanced matrix mineralization (PINP and OCN levels) in CSE-induced bone cells by switching to upregulation of OPG. Furthermore, the protective effects of Mg supplementation were more pronounced at 4 mM than at 1 mM.

Based on these findings, Mg supplementation may be an effective strategy to prevent or treat osteoporotic bones in smokers. When patients are found to have Mg deficiency, Mg supplementation can be administered orally or intravenously to prevent or treat osteoporotic bones, especially for smokers. Further clinical studies are required to clarify the Mg administration patterns, such as dose and duration.

6. Zusammenfassung

Es ist allgemein bekannt, dass CS einen negativen Einfluss auf die Knochenhomöostase hat und damit zu einem erhöhten Risiko für Fragilitätsfrakturen und einer beeinträchtigten Frakturheilung beiträgt. In vorrausgehenden Studien konnte gezeigt werden, dass CS sowohl die Osteoblastenaktivität unterdrückt als auch die Osteoklastenaktivität erhöht.

Mg fördert die osteogenen Differenzierung osteoblastärer Vorläuferzellen und unterdrückt die Differenzierung osteoklastärer Vorläuferzellen, weshalb es nicht überraschen ist, dass ein Mg-Mangel mit Knochenschwund in Verbindung gebracht werden kann. Eine klinische Studies konnte zeigen, dass, im Vergleich zu Nichtrauchern, starke Raucher einen bemerkenswert niedrigeren Mg-Serumspiegel aufwiesen. Darauf basierend, stellen wir die Hypothese auf, dass durch eine Supplementierung mit Mg, die negativen Auswirkungen von CS auf den Knochenstoffwechsel aufgehoben werden können.

Um die reparative Phase der Knochenheilung *in vitro* so authentisch wie möglich nachzustellen, wurde in dieser Studie ein *In-vitro* Knochen-Kokulturmodell, bestehend aus SCP-1-Zellen (Osteoprogenitorzellen) und THP-1-Zellen (osteoklastären Vorläuferzellen) kokultiviert auf einem GEL-Scaffold, etabliert. Wir untersuchten dann, die Auswirkungen einer Mg-Supplementierung auf das durch CSE beeinträchtigte 3D-Knochen-Kokultursystem. Wir konnten beobachteten, dass 5 % CSE die Differenzierung von Osteoklasten aus THP-1-Zellen verstärkte und die osteogene Differenzierung von SCP-1-Zellen hemmte, wodurch eine osteoporotische Mikroumgebung entstand, sowie sie auch bei Rauchern beobachtet werden kann. Die Zugabe von 4 mM Mg hemmte effektiv die Funktionalität der Osteoklasen (TRAP- und CAII-Aktivitäten) und verbesserte die Matrixmineralisierung (PINP- und OCN-Protein Levels) in CSE stimulierten Knochenzellen. Als Grund dafür konnten höherer OPG Level identifiziert werden. Desweitern ware die schützende Wirkung von Mg durch die höhrern Konzentrationen von 4 mM ausgeprägter als wenn nur 1 mM verwendet wurde.

Die Supplementatierung mit Mg kann, basierend auf unseren Ergebnissen, eine wirksame Strategie zur Vorbeugung oder Behandlung osteoporotischer Knochen bei Rauchern sein. Sollte eine Mg Mangel bei Patienten festgestelle werden, kann eine Mg-Supplementierung kann sowohl oral oder intravenös verabreicht werden. Weitere klinische Studien sind jedoch nötig um Mg-Verabreichungsmuster, wie Dosis oder Dauer, zu präzisieren.

7. Bibliography

AKHTER, M. P., IWANIEC, U. T., HAYNATZKI, G. R., FUNG, Y. K., CULLEN, D. M. & RECKER, R. R. 2003. Effects of nicotine on bone mass and strength in aged female rats. *J Orthop Res,* 21**,** 14-9.

ALFORD, A. I., KOZLOFF, K. M. & HANKENSON, K. D. 2015. Extracellular matrix networks in bone remodeling. *Int J Biochem Cell Biol,* 65**,** 20-31.

ALHOSAINI, M. & LEEHEY, D. J. 2015. Magnesium and Dialysis: The Neglected Cation. *Am J Kidney Dis,* 66**,** 523-31.

ANDREW, J. G., HOYLAND, J. A., FREEMONT, A. J. & MARSH, D. R. 1995. Platelet-derived growth factor expression in normally healing human fractures. *Bone,* 16**,** 455-60.

ASPERA-WERZ, R. H., CHEN, T., EHNERT, S., ZHU, S., FRÖHLICH, T. & NUSSLER, A. K. 2019. Cigarette Smoke Induces the Risk of Metabolic Bone Diseases: Transforming Growth Factor Beta Signaling Impairment via Dysfunctional Primary Cilia Affects Migration, Proliferation, and Differentiation of Human Mesenchymal Stem Cells. *Int J Mol Sci,* 20.

ASPERA-WERZ, R. H., EHNERT, S., HEID, D., ZHU, S., CHEN, T., BRAUN, B., SREEKUMAR, V., ARNSCHEIDT, C. & NUSSLER, A. K. 2018. Nicotine and Cotinine Inhibit Catalase and Glutathione Reductase Activity Contributing to the Impaired Osteogenesis of SCP-1 Cells Exposed to Cigarette Smoke. *Oxid Med Cell Longev,* 2018**,** 3172480.

ASPERA-WERZ, R. H., EHNERT, S., MÜLLER, M., ZHU, S., CHEN, T., WENG, W., JACOBY, J. & NUSSLER, A. K. 2020. Assessment of tobacco heating system 2.4 on osteogenic differentiation of mesenchymal stem cells and primary human osteoblasts compared to conventional cigarettes. *World J Stem Cells,* 12**,** 841-856.

ATA, M. A., SHAIKH, S. S., IQBAL, T., HINA, JAMIL, D., KHAN, R., QAZI, M. B. & RIWAN, T. 2015. Inverse Correlation between Serum C-Reactive Protein and Magnesium Levels in Smokers and Nonsmokers. *N Am J Med Sci,* 7**,** 271-4.

BAE, Y. J. & KIM, M. H. 2010. Calcium and Magnesium Supplementation Improves Serum OPG/RANKL in Calcium-Deficient Ovariectomized Rats. *Calcif Tissue Int,* 87**,** 365-72.

BAHNEY, C. S., HU, D. P., MICLAU, T., 3RD & MARCUCIO, R. S. 2015. The multifaceted role of the vasculature in endochondral fracture repair. *Front Endocrinol (Lausanne),* 6**,** 4.

BARBAGALLO, M., VERONESE, N. & DOMINGUEZ, L. J. 2021. Magnesium in aging, health and diseases. *Nutrients,* 13**,** 463.

BENOWITZ, N. L. 2008. Clinical pharmacology of nicotine: implications for understanding, preventing, and treating tobacco addiction. *Clin Pharmacol Ther,* 83**,** 531-41.

BERGLUND, A. K., LONG, J. M., ROBERTSON, J. B. & SCHNABEL, L. V. 2021.

TGF-β2 Reduces the Cell-Mediated Immunogenicity of Equine MHC-Mismatched Bone Marrow-Derived Mesenchymal Stem Cells Without Altering Immunomodulatory Properties. *Front Cell Dev Biol,* 9**,** 628382.

BERNHARDT, A., LODE, A., PETERS, F. & GELINSKY, M. 2011. Novel ceramic bone replacement material Osbone® in a comparative in vitro study with osteoblasts. *Clin Oral Implants Res,* 22**,** 651-7.

BIAN, J., CAO, D., SHEN, J., JIANG, B., CHEN, D. & BIAN, L. 2018. N-methyl pyrrolidone promotes ankle fracture healing by inhibiting inflammation via suppression of the mitogen-activated protein kinase signaling pathway. *Exp Ther Med,* 15**,** 3617-3622.

BOCKER, W., YIN, Z., DROSSE, I., HAASTERS, F., ROSSMANN, O., WIERER, M., POPOV, C., LOCHER, M., MUTSCHLER, W., DOCHEVA, D. & SCHIEKER, M. 2008. Introducing a single-cell-derived human mesenchymal stem cell line expressing hTERT after lentiviral gene transfer. *J Cell Mol Med,* 12**,** 1347-59.

BOSTROM, M. P., LANE, J. M., BERBERIAN, W. S., MISSRI, A. A., TOMIN, E., WEILAND, A., DOTY, S. B., GLASER, D. & ROSEN, V. M. 1995. Immunolocalization and expression of bone morphogenetic proteins 2 and 4 in fracture healing. *J Orthop Res,* 13**,** 357-67.

BOULETREAU, P. J., WARREN, S. M., SPECTOR, J. A., PELED, Z. M., GERRETS, R. P., GREENWALD, J. A. & LONGAKER, M. T. 2002. Hypoxia and VEGF up-regulate BMP-2 mRNA and protein expression in microvascular endothelial cells: implications for fracture healing. *Plast Reconstr Surg,* 109**,** 2384-97.

BOURGINE, P. E., SCOTTI, C., PIGEOT, S., TCHANG, L. A., TODOROV, A. & MARTIN, I. 2014. Osteoinductivity of engineered cartilaginous templates devitalized by inducible apoptosis. *Proc Natl Acad Sci U S A,* 111**,** 17426-31.

BOYCE, B. F. & XING, L. 2008. Functions of RANKL/RANK/OPG in bone modeling and remodeling. *Arch Biochem Biophys,* 473**,** 139-46.

BUZA, J. A., 3RD & EINHORN, T. 2016. Bone healing in 2016. *Clin Cases Miner Bone Metab,* 13**,** 101-105.

CARRILLO-LÓPEZ, N., MARTÍNEZ-ARIAS, L., FERNÁNDEZ-VILLABRILLE, S., RUIZ-TORRES, M. P., DUSSO, A., CANNATA-ANDÍA, J. B., NAVES-DÍAZ, M. & PANIZO, S. 2021. Role of the RANK/RANKL/OPG and Wnt/β-Catenin Systems in CKD Bone and Cardiovascular Disorders. *Calcif Tissue Int,* 108**,** 439-451.

CHEN, M., HAN, H., ZHOU, S., WEN, Y. & CHEN, L. 2021. Morusin induces osteogenic differentiation of bone marrow mesenchymal stem cells by canonical Wnt/β-catenin pathway and prevents bone loss in an ovariectomized rat model. *Stem Cell Res Ther,* 12**,** 173.

CHENG, C. & SHOBACK, D. 2019. Mechanisms Underlying Normal Fracture Healing and Risk Factors for Delayed Healing. *Curr Osteoporos Rep,* 17**,** 36-47.

CHO, T. J., KIM, J. A., CHUNG, C. Y., YOO, W. J., GERSTENFELD, L. C., EINHORN, T. A. & CHOI, I. H. 2007. Expression and role of interleukin-6 in distraction osteogenesis. *Calcif Tissue Int,* 80**,** 192-200.

CHOI, H. K., KIM, G. J., YOO, H. S., SONG, D. H., CHUNG, K. H., LEE, K. J., KOO, Y. T. & AN, J. H. 2019. Vitamin C Activates Osteoblastogenesis and Inhibits Osteoclastogenesis via Wnt/β-Catenin/ATF4 Signaling Pathways. *Nutrients,* 11.

CHRISTENSEN, J. & SHASTRI, V. P. 2015. Matrix-metalloproteinase-9 is cleaved and activated by cathepsin K. *BMC Res Notes,* 8**,** 322.

CHU, M., SUN, Z., FAN, Z., YU, D., MAO, Y. & GUO, Y. 2021. Bi-directional regulation functions of lanthanum-substituted layered double hydroxide nanohybrid scaffolds via activating osteogenesis and inhibiting osteoclastogenesis for osteoporotic bone regeneration. *Theranostics,* 11**,** 6717-6734.

CLAES, L., RECKNAGEL, S. & IGNATIUS, A. 2012. Fracture healing under healthy and inflammatory conditions. *Nat Rev Rheumatol,* 8**,** 133-43.

CLÉZARDIN, P., COLEMAN, R., PUPPO, M., OTTEWELL, P., BONNELYE, E., PAYCHA, F., CONFAVREUX, C. B. & HOLEN, I. 2021. Bone metastasis: mechanisms, therapies, and biomarkers. *Physiol Rev,* 101**,** 797-855.

CROTTI, T. N., O'SULLIVAN, R. P., SHEN, Z., FLANNERY, M. R., FAJARDO, R. J., ROSS, F. P., GOLDRING, S. R. & MCHUGH, K. P. 2011. Bone matrix regulates osteoclast differentiation and annexin A8 gene expression. *J Cell Physiol,* 226**,** 3413-21.

CUI, Q., LI, N., NIE, F., YANG, F., LI, H. & ZHANG, J. 2021. Vitamin K2 promotes the osteogenic differentiation of periodontal ligament stem cells via the Wnt/β-catenin signaling pathway. *Arch Oral Biol,* 124**,** 105057.

DELAISSE, J. M., ANDERSEN, T. L., ENGSIG, M. T., HENRIKSEN, K., TROEN, T. & BLAVIER, L. 2003. Matrix metalloproteinases (MMP) and cathepsin K contribute differently to osteoclastic activities. *Microsc Res Tech,* 61**,** 504-13.

DI MAGGIO, N., PICCININI, E., JAWORSKI, M., TRUMPP, A., WENDT, D. J. & MARTIN, I. 2011. Toward modeling the bone marrow niche using scaffold-based 3D culture systems. *Biomaterials,* 32**,** 321-9.

DUCY, P., DESBOIS, C., BOYCE, B., PINERO, G., STORY, B., DUNSTAN, C., SMITH, E., BONADIO, J., GOLDSTEIN, S., GUNDBERG, C., BRADLEY, A. & KARSENTY, G. 1996. Increased bone formation in osteocalcin-deficient mice. *Nature,* 382**,** 448-52.

DUELLMAN, T., WARREN, C. L., PEISSIG, P., WYNN, M. & YANG, J. 2012. Matrix metalloproteinase-9 genotype as a potential genetic marker for abdominal aortic aneurysm. *Circ Cardiovasc Genet,* 5**,** 529-37.

DURLACH, J., GUIET-BARA, A., PAGÈS, N., BAC, P. & BARA, M. 2005. Magnesium chloride or magnesium sulfate: a genuine question. *Magnesium research,* 18**,** 187-192.

EHNERT, S., ASPERA-WERZ, R. H., IHLE, C., TROST, M., ZIRN, B., FLESCH, I., SCHRÖTER, S., RELJA, B. & NUSSLER, A. K. 2019. Smoking Dependent Alterations in Bone Formation and Inflammation Represent Major Risk Factors for Complications Following Total Joint Arthroplasty. *J Clin Med,* 8.

EHNERT, S., RELJA, B., SCHMIDT-BLEEK, K., FISCHER, V., IGNATIUS, A., LINNEMANN, C., RINDERKNECHT, H., HUBER-LANG, M., KALBITZ, M.

& HISTING, T. 2021. Effects of immune cells on mesenchymal stem cells during fracture healing. *World Journal of Stem Cells,* 13**,** 1667.

EHNERT, S., RINDERKNECHT, H., ASPERA-WERZ, R. H., HÄUSSLING, V. & NUSSLER, A. K. 2020. Use of in vitro bone models to screen for altered bone metabolism, osteopathies, and fracture healing: challenges of complex models. *Arch Toxicol,* 94**,** 3937-3958.

EHNERT, S., SEELIGER, C., VESTER, H., SCHMITT, A., SAIDY-RAD, S., LIN, J., NEUMAIER, M., GILLEN, S., KLEEFF, J., FRIESS, H., BURKHART, J., STÖCKLE, U. & NÜSSLER, A. K. 2011. Autologous serum improves yield and metabolic capacity of monocyte-derived hepatocyte-like cells: possible implication for cell transplantation. *Cell Transplant,* 20**,** 1465-77.

ELANGO, J., ROBINSON, J., ZHANG, J., BAO, B., MA, N., DE VAL, J. & WU, W. 2019. Collagen Peptide Upregulates Osteoblastogenesis from Bone Marrow Mesenchymal Stem Cells through MAPK- Runx2. *Cells,* 8.

ENGLER, A. J., SEN, S., SWEENEY, H. L. & DISCHER, D. E. 2006. Matrix elasticity directs stem cell lineage specification. *Cell,* 126**,** 677-89.

ENGSIG, M. T., CHEN, Q. J., VU, T. H., PEDERSEN, A. C., THERKIDSEN, B., LUND, L. R., HENRIKSEN, K., LENHARD, T., FOGED, N. T., WERB, Z. & DELAISSÉ, J. M. 2000. Matrix metalloproteinase 9 and vascular endothelial growth factor are essential for osteoclast recruitment into developing long bones. *J Cell Biol,* 151**,** 879-89.

ESPOSITO, M., FANG, C., COOK, K. C., PARK, N., WEI, Y., SPADAZZI, C., BRACHA, D., GUNARATNA, R. T., LAEVSKY, G., DECOSTE, C. J., SLABODKIN, H., BRANGWYNNE, C. P., CRISTEA, I. M. & KANG, Y. 2021. TGF-β-induced DACT1 biomolecular condensates repress Wnt signalling to promote bone metastasis. *Nature cell biology,* 23**,** 257-267.

FANG, T. D., SALIM, A., XIA, W., NACAMULI, R. P., GUCCIONE, S., SONG, H. M., CARANO, R. A., FILVAROFF, E. H., BEDNARSKI, M. D., GIACCIA, A. J. & LONGAKER, M. T. 2005. Angiogenesis is required for successful bone induction during distraction osteogenesis. *J Bone Miner Res,* 20**,** 1114-24.

FEI, C., GUO, J., ZHAO, Y., GU, S., ZHAO, S., LI, X. & CHANG, C. 2015. Notch-Hes pathway mediates the impaired osteogenic differentiation of bone marrow mesenchymal stromal cells from myelodysplastic syndromes patients through the down-regulation of Runx2. *Am J Transl Res,* 7**,** 1939-51.

FILIPPI, M., BORN, G., CHAABAN, M. & SCHERBERICH, A. 2020. Natural Polymeric Scaffolds in Bone Regeneration. *Front Bioeng Biotechnol,* 8**,** 474.

FIORENTINI, D., CAPPADONE, C., FARRUGGIA, G. & PRATA, C. 2021. Magnesium: biochemistry, nutrition, detection, and social impact of diseases linked to its deficiency. *Nutrients,* 13**,** 1136.

FLORENCIO-SILVA, R., SASSO, G. R., SASSO-CERRI, E., SIMÕES, M. J. & CERRI, P. S. 2015. Biology of Bone Tissue: Structure, Function, and Factors That Influence Bone Cells. *Biomed Res Int,* 2015**,** 421746.

FREUDENHEIM, J. L., JOHNSON, N. E. & SMITH, E. L. 1986. Relationships between usual nutrient intake and bone-mineral content of women 35-65 years

of age: longitudinal and cross-sectional analysis. *Am J Clin Nutr,* 44**,** 863-76.

FUJITA, M., CHENG, X. W., INDEN, Y., SHIMANO, M., YOSHIDA, N., INOUE, A., YAMAMOTO, T., TAKESHITA, K., KYO, S., TAGUCHI, N., SHI, G. P., KUZUYA, M., OKUMURA, K. & MUROHARA, T. 2013. Mechanisms with clinical implications for atrial fibrillation-associated remodeling: cathepsin K expression, regulation, and therapeutic target and biomarker. *J Am Heart Assoc,* 2**,** e000503.

GENTILI, C. & CANCEDDA, R. 2009. Cartilage and bone extracellular matrix. *Curr Pharm Des,* 15**,** 1334-48.

GHIASI, M. S., CHEN, J., VAZIRI, A., RODRIGUEZ, E. K. & NAZARIAN, A. 2017. Bone fracture healing in mechanobiological modeling: A review of principles and methods. *Bone Rep,* 6**,** 87-100.

GLASS, D. A., 2ND, BIALEK, P., AHN, J. D., STARBUCK, M., PATEL, M. S., CLEVERS, H., TAKETO, M. M., LONG, F., MCMAHON, A. P., LANG, R. A. & KARSENTY, G. 2005. Canonical Wnt signaling in differentiated osteoblasts controls osteoclast differentiation. *Dev Cell,* 8**,** 751-64.

GOMEZ-BARRENA, E., ROSSET, P., LOZANO, D., STANOVICI, J., ERMTHALLER, C. & GERBHARD, F. 2015. Bone fracture healing: cell therapy in delayed unions and nonunions. *Bone,* 70**,** 93-101.

GRANERO-MOLTO, F., WEIS, J. A., MIGA, M. I., LANDIS, B., MYERS, T. J., O'REAR, L., LONGOBARDI, L., JANSEN, E. D., MORTLOCK, D. P. & SPAGNOLI, A. 2009. Regenerative effects of transplanted mesenchymal stem cells in fracture healing. *Stem Cells,* 27**,** 1887-98.

GULER, E., BARIPOGLU, Y. E., ALENEZI, H., ARIKAN, A., BABAZADE, R., UNAL, S., DURUKSU, G., ALFARES, F. S., YAZIR, Y., OKTAR, F. N., GUNDUZ, O., EDIRISINGHE, M. & CAM, M. E. 2021. Vitamin D(3)/vitamin K(2)/magnesium-loaded polylactic acid/tricalcium phosphate/polycaprolactone composite nanofibers demonstrated osteoinductive effect by increasing Runx2 via Wnt/β-catenin pathway. *Int J Biol Macromol,* 190**,** 244-258.

GUO, A., LI, K., TIAN, H. C., TAO, B. L., XIAO, Q. & JIANG, D. M. 2022. FGF19 protects against obesity-induced bone loss by promoting osteogenic differentiation. *Biomed Pharmacother,* 146**,** 112524.

HADJIDAKIS, D. J. & ANDROULAKIS, II 2006. Bone remodeling. *Ann N Y Acad Sci,* 1092**,** 385-96.

HARRIS, A. S., ESTANDÍA, A., SMITH, H. T., OLSEN, R. W., FORD JR, T. J. & TILLOTSON, R. F. 1952. Magnesium sulfate and chloride in suppression of ectopic ventricular tachycardia accompanying acute myocardial infarction. *American Journal of Physiology-Legacy Content,* 172**,** 251-258.

HÄUSSLING, V., ASPERA-WERZ, R. H., RINDERKNECHT, H., SPRINGER, F., ARNSCHEIDT, C., MENGER, M. M., HISTING, T., NUSSLER, A. K. & EHNERT, S. 2021. 3D Environment Is Required In Vitro to Demonstrate Altered Bone Metabolism Characteristic for Type 2 Diabetics. *Int J Mol Sci,* 22.

HE, B., HU, M., LI, S. D., YANG, X. T., LU, Y. Q., LIU, J. X., CHEN, P. & SHEN, Z. Q. 2013. Effects of geraniin on osteoclastic bone resorption and matrix

metalloproteinase-9 expression. *Bioorg Med Chem Lett,* 23**,** 630-4.
HODGE, J. M., COLLIER, F. M., PAVLOS, N. J., KIRKLAND, M. A. & NICHOLSON, G. C. 2011. M-CSF potently augments RANKL-induced resorption activation in mature human osteoclasts. *PLoS One,* 6**,** e21462.
HUEBSCH, N., ARANY, P. R., MAO, A. S., SHVARTSMAN, D., ALI, O. A., BENCHERIF, S. A., RIVERA-FELICIANO, J. & MOONEY, D. J. 2010. Harnessing traction-mediated manipulation of the cell/matrix interface to control stem-cell fate. *Nat Mater,* 9**,** 518-26.
HUNG, C. C., CHAYA, A., LIU, K., VERDELIS, K. & SFEIR, C. 2019. The role of magnesium ions in bone regeneration involves the canonical Wnt signaling pathway. *Acta Biomater,* 98**,** 246-255.
HYNES, R. O. 2009. The extracellular matrix: not just pretty fibrils. *Science,* 326**,** 1216-9.
IMAMURA, A., KAJIYA, H., FUJISAKI, S., MAESHIBA, M., YANAGI, T., KOJIMA, H. & OHNO, J. 2020. Three-dimensional spheroids of mesenchymal stem/stromal cells promote osteogenesis by activating stemness and Wnt/β-catenin. *Biochem Biophys Res Commun,* 523**,** 458-464.
INFANTE, A. & RODRIGUEZ, C. I. 2018. Osteogenesis and aging: lessons from mesenchymal stem cells. *Stem Cell Res Ther,* 9**,** 244.
JANSEN, I. D., VERMEER, J. A., BLOEMEN, V., STAP, J. & EVERTS, V. 2012. Osteoclast fusion and fission. *Calcif Tissue Int,* 90**,** 515-22.
JI, W. & SUN, X. 2022. Methyl-CpG-binding protein 2 promotes osteogenic differentiation of bone marrow mesenchymal stem cells through regulating forkhead box F1/Wnt/β-Catenin axis. *Bioengineered,* 13**,** 583-592.
KARSENTY, G. 2000. The central regulation of bone remodeling. *Trends Endocrinol Metab,* 11**,** 437-9.
KARSENTY, G. & WAGNER, E. F. 2002. Reaching a genetic and molecular understanding of skeletal development. *Dev Cell,* 2**,** 389-406.
KEBIR, N. E. & ZAHZEH, T. 2022. Magnesium Deficiency Associated with Stress, Systemic Inflammation, and Insulin Resistance in Diabetes Mellitus: a review. *Egyptian Academic Journal of Biological Sciences. C, Physiology and Molecular Biology,* 14**,** 31-46.
KHAND, F., SHAIKH, S. S., ATA, M. A. & SHAIKH, S. S. 2015. Evaluation of the effect of smoking on complete blood counts, serum C-reactive protein and magnesium levels in healthy adult male smokers. *J Pak Med Assoc,* 65**,** 59-61.
KIM, J. A., YUN, H. S., CHOI, Y. A., KIM, J. E., CHOI, S. Y., KWON, T. G., KIM, Y. K., KWON, T. Y., BAE, M. A., KIM, N. J., BAE, Y. C., SHIN, H. I. & PARK, E. K. 2018. Magnesium phosphate ceramics incorporating a novel indene compound promote osteoblast differentiation in vitro and bone regeneration in vivo. *Biomaterials,* 157**,** 51-61.
KO, C. H., CHAN, R. L., SIU, W. S., SHUM, W. T., LEUNG, P. C., ZHANG, L. & CHO, C. H. 2015. Deteriorating effect on bone metabolism and microstructure by passive cigarette smoking through dual actions on osteoblast and osteoclast. *Calcif Tissue Int,* 96**,** 389-400.

KOLAR, P., GABER, T., PERKA, C., DUDA, G. N. & BUTTGEREIT, F. 2011. Human early fracture hematoma is characterized by inflammation and hypoxia. *Clin Orthop Relat Res,* 469**,** 3118-26.

KON, T., CHO, T. J., AIZAWA, T., YAMAZAKI, M., NOOH, N., GRAVES, D., GERSTENFELD, L. C. & EINHORN, T. A. 2001. Expression of osteoprotegerin, receptor activator of NF-kappaB ligand (osteoprotegerin ligand) and related proinflammatory cytokines during fracture healing. *J Bone Miner Res,* 16**,** 1004-14.

KONG, Y., HU, X., ZHONG, Y., XU, K., WU, B. & ZHENG, J. 2019. Magnesium-enriched microenvironment promotes odontogenic differentiation in human dental pulp stem cells by activating ERK/BMP2/Smads signaling. *Stem Cell Res Ther,* 10**,** 378.

KRISHNAKUMAR, G. S., SAMPATH, S., MUTHUSAMY, S. & JOHN, M. A. 2019. Importance of crosslinking strategies in designing smart biomaterials for bone tissue engineering: A systematic review. *Mater Sci Eng C Mater Biol Appl,* 96**,** 941-954.

KRISHNAN, V., BRYANT, H. U. & MACDOUGALD, O. A. 2006. Regulation of bone mass by Wnt signaling. *J Clin Invest,* 116**,** 1202-9.

KULAR, J., TICKNER, J., CHIM, S. M. & XU, J. 2012. An overview of the regulation of bone remodelling at the cellular level. *Clin Biochem,* 45**,** 863-73.

LECKA-CZERNIK, B. 2017. Diabetes, bone and glucose-lowering agents: basic biology. *Diabetologia,* 60**,** 1163-1169.

LEWIS, A., MILLER, J. H. & LEA, R. A. 2007. Monoamine oxidase and tobacco dependence. *Neurotoxicology,* 28**,** 182-95.

LI, H., LIU, Y., XING, L., YANG, X., XU, J., REN, Q., SU, K. P., LU, Y. & WANG, F. 2020. Association of Cigarette Smoking with Sleep Disturbance and Neurotransmitters in Cerebrospinal Fluid. *Nat Sci Sleep,* 12**,** 801-808.

LI, M., WAN, P., WANG, W., YANG, K., ZHANG, Y. & HAN, Y. 2019. Regulation of osteogenesis and osteoclastogenesis by zoledronic acid loaded on biodegradable magnesium-strontium alloy. *Sci Rep,* 9**,** 933.

LI, Y., XING, B. X., WANG, Y. H., YU, S., ZHAO, H., LV, Q. Q. & LU, C. X. 2022. CTHRC1 promotes growth, migration and invasion of trophoblasts via reciprocal Wnt/β-catenin regulation. *J Cell Commun Signal,* 16**,** 63-74.

LIN, S., YANG, G., JIANG, F., ZHOU, M., YIN, S., TANG, Y., TANG, T., ZHANG, Z., ZHANG, W. & JIANG, X. 2019. A Magnesium-Enriched 3D Culture System that Mimics the Bone Development Microenvironment for Vascularized Bone Regeneration. *Adv Sci (Weinh),* 6**,** 1900209.

LISSENBERG-THUNNISSEN, S. N., DE GORTER, D. J., SIER, C. F. & SCHIPPER, I. B. 2011. Use and efficacy of bone morphogenetic proteins in fracture healing. *Int Orthop,* 35**,** 1271-80.

LIU, H., GUO, Y., ZHU, R., WANG, L., CHEN, B., TIAN, Y., LI, R., MA, R., JIA, Q., ZHANG, H., XIA, B., LI, Y., WANG, X., ZHU, X., ZHANG, R., BRÖMME, D., GAO, S., ZHANG, D. & PEI, X. 2021. Fructus Ligustri Lucidi preserves bone quality through induction of canonical Wnt/β-catenin signaling pathway

in ovariectomized rats. *Phytother Res,* 35**,** 424-441.

LIU, J., QI, X., WANG, X. H., MIAO, H. S., XUE, Z. C., ZHANG, L. L., ZHAO, S. H., WU, L. H., GAO, G. Y., LOU, M. Q. & YI, C. Q. 2022. Downregulation of the LncRNA MEG3 Promotes Osteogenic Differentiation of BMSCs and Bone Repairing by Activating Wnt/β-Catenin Signaling Pathway. *J Clin Med,* 11.

LIU, J., XIAO, Q., XIAO, J., NIU, C., LI, Y., ZHANG, X., ZHOU, Z., SHU, G. & YIN, G. 2022. Wnt/β-catenin signalling: function, biological mechanisms, and therapeutic opportunities. *Signal Transduct Target Ther,* 7**,** 3.

LIU, Y., COOPER, P. R., BARRALET, J. E. & SHELTON, R. M. 2007. Influence of calcium phosphate crystal assemblies on the proliferation and osteogenic gene expression of rat bone marrow stromal cells. *Biomaterials,* 28**,** 1393-403.

LIU, Y., WANG, Y., YUAN, W., DONG, F., ZHEN, F., LIU, J., YANG, L., QU, X. & YAO, R. 2021. Reelin promotes oligodendrocyte precursors migration via the Wnt/β-catenin signaling pathway. *Neurol Res,* 43**,** 543-552.

LYNCH, J. R., TAITSMAN, L. A., BAREI, D. P. & NORK, S. E. 2008. Femoral nonunion: risk factors and treatment options. *J Am Acad Orthop Surg,* 16**,** 88-97.

MAHDAVI-ROSHAN, M., EBRAHIMI, M. & EBRAHIMI, A. 2015. Copper, magnesium, zinc and calcium status in osteopenic and osteoporotic post-menopausal women. *Clin Cases Miner Bone Metab,* 12**,** 18-21.

MAMMOLI, F., CASTIGLIONI, S., PARENTI, S., CAPPADONE, C., FARRUGGIA, G., IOTTI, S., DAVALLI, P., MAIER, J. A., GRANDE, A. & FRASSINETI, C. 2019. Magnesium is a key regulator of the balance between osteoclast and osteoblast differentiation in the presence of vitamin D3. *International journal of molecular sciences,* 20**,** 385.

MARIA, S. M., PRUKNER, C., SHEIKH, Z., MUELLER, F., BARRALET, J. E. & KOMAROVA, S. V. 2014. Reproducible quantification of osteoclastic activity: characterization of a biomimetic calcium phosphate assay. *J Biomed Mater Res B Appl Biomater,* 102**,** 903-12.

MARIN, C., LUYTEN, F. P., VAN DER SCHUEREN, B., KERCKHOFS, G. & VANDAMME, K. 2018. The Impact of Type 2 Diabetes on Bone Fracture Healing. *Front Endocrinol (Lausanne),* 9**,** 6.

MAZUR, A., MAIER, J. A., ROCK, E., GUEUX, E., NOWACKI, W. & RAYSSIGUIER, Y. 2007. Magnesium and the inflammatory response: potential physiopathological implications. *Arch Biochem Biophys,* 458**,** 48-56.

MEHTA, M., SCHMIDT-BLEEK, K., DUDA, G. N. & MOONEY, D. J. 2012. Biomaterial delivery of morphogens to mimic the natural healing cascade in bone. *Adv Drug Deliv Rev,* 64**,** 1257-76.

MENG, S.-H., WANG, M.-X., KANG, L.-X., FU, J.-M., ZHOU, H.-B., LI, X., LI, X., LI, X.-T. & ZHAO, Y.-S. 2021. Dietary intake of calcium and magnesium in relation to severe headache or migraine. *Frontiers in Nutrition,* 8**,** 83.

MIAO, W., GAO, H. & HOU, X. 2019. Magnesium lithospermate B inhibits titanium particles-induced osteoclast formation by c-fos and inhibiting NFATc1 expression. *Connect Tissue Res,* 60**,** 487-494.

MIECZKOWSKI, M., MATUSZKIEWICZ-ROWIŃSKA, J. & KOSCIELSKA, M. 2013. [Magnesium homeostasis]. *Wiad Lek,* 66**,** 311-3.

MILLS, L. A., AITKEN, S. A. & SIMPSON, A. 2017. The risk of non-union per fracture: current myths and revised figures from a population of over 4 million adults. *Acta Orthop,* 88**,** 434-439.

MOGHADDAM, A., WEISS, S., WÖLFL, C. G., SCHMECKENBECHER, K., WENTZENSEN, A., GRÜTZNER, P. A. & ZIMMERMANN, G. 2010. Cigarette smoking decreases TGF-b1 serum concentrations after long bone fracture. *Injury,* 41**,** 1020-5.

MURRAY, I. R., FOSTER, C. J., EROS, A. & ROBINSON, C. M. 2013. Risk factors for nonunion after nonoperative treatment of displaced midshaft fractures of the clavicle. *J Bone Joint Surg Am,* 95**,** 1153-8.

NAIR, M., NANCY, D., KRISHNAN, A. G., ANJUSREE, G. S., VADUKUMPULLY, S. & NAIR, S. V. 2015. Graphene oxide nanoflakes incorporated gelatin-hydroxyapatite scaffolds enhance osteogenic differentiation of human mesenchymal stem cells. *Nanotechnology,* 26**,** 161001.

NANKO, N., TANIKAWA, M., MASE, M., FUJITA, M., TATEYAMA, H., MIYATI, T. & YAMADA, K. 2009. Involvement of hypoxia-inducible factor-1alpha and vascular endothelial growth factor in the mechanism of development of chronic subdural hematoma. *Neurol Med Chir (Tokyo),* 49**,** 379-85.

NEMMAR, A., BEEGAM, S., YUVARAJU, P., YASIN, J., ALI, B. H. & ADEGHATE, E. 2020. Nose-Only Water-Pipe Smoke Exposure in Mice Elicits Renal Histopathological Alterations, Inflammation, Oxidative Stress, DNA Damage, and Apoptosis. *Front Physiol,* 11**,** 46.

NI, S., XIONG, X. B. & NI, X. Y. 2020. MgCl2 promotes mouse mesenchymal stem cell osteogenic differentiation by activating the p38/Osx/Runx2 signaling pathway. *Mol Med Rep,* 22**,** 3904-3910.

NIJWEIDE, P. J., BURGER, E. H. & FEYEN, J. H. 1986. Cells of bone: proliferation, differentiation, and hormonal regulation. *Physiol Rev,* 66**,** 855-86.

NISHINO, K., TAMAI, K., ORITA, K., HASHIMOTO, Y. & NAKAMURA, H. 2021. Heated Tobacco Products Impair Cell Viability, Osteoblastic Differentiation, and Bone Fracture-Healing. *J Bone Joint Surg Am,* 103**,** 2024-2031.

O'KEEFFE, L. M., TAYLOR, G., HUXLEY, R. R., MITCHELL, P., WOODWARD, M. & PETERS, S. A. E. 2018. Smoking as a risk factor for lung cancer in women and men: a systematic review and meta-analysis. *BMJ Open,* 8**,** e021611.

OHGUSHI, H., MIYAKE, J. & TATEISHI, T. 2003. Mesenchymal stem cells and bioceramics: strategies to regenerate the skeleton. *Novartis Found Symp,* 249**,** 118-27; discussion 127-32, 170-4, 239-41.

ORTEGA, N., BEHONICK, D. J. & WERB, Z. 2004. Matrix remodeling during endochondral ossification. *Trends Cell Biol,* 14**,** 86-93.

PANZAVOLTA, S., TORRICELLI, P., CASOLARI, S., PARRILLI, A., FINI, M. & BIGI, A. 2018. Strontium-Substituted Hydroxyapatite-Gelatin Biomimetic Scaffolds Modulate Bone Cell Response. *Macromol Biosci,* 18**,** e1800096.

PAOLISSO, G., SCHEEN, A., D'ONOFRIO, F. & LEFÈBVRE, P. 1990. Magnesium

and glucose homeostasis. *Diabetologia,* 33**,** 511-4.
PINHO, L. C., GARBIERI, T. F., GRENHO, L., ALVES, M. M., SOUSA GOMES, P., SANTOS, C. F., FERNANDES, M. H., SANTOS, C. & COLACO, B. 2021. Rosehip Extract-Functionalized Magnesium Hydroxide Nanoparticles and Its Effect on Osteoblastic and Osteoclastic Cells. *Materials (Basel),* 14.
PITTENGER, M. F., MACKAY, A. M., BECK, S. C., JAISWAL, R. K., DOUGLAS, R., MOSCA, J. D., MOORMAN, M. A., SIMONETTI, D. W., CRAIG, S. & MARSHAK, D. R. 1999. Multilineage potential of adult human mesenchymal stem cells. *Science,* 284**,** 143-7.
PROCHASKA, J. J. & BENOWITZ, N. L. 2019. Current advances in research in treatment and recovery: Nicotine addiction. *Sci Adv,* 5**,** eaay9763.
PROVOT, S. & SCHIPANI, E. 2005. Molecular mechanisms of endochondral bone development. *Biochem Biophys Res Commun,* 328**,** 658-65.
QI, T., WENG, J., YU, F., ZHANG, W., LI, G., QIN, H., TAN, Z. & ZENG, H. 2021. Insights into the Role of Magnesium Ions in Affecting Osteogenic Differentiation of Mesenchymal Stem Cells. *Biol Trace Elem Res,* 199**,** 559-567.
QIANG, Y. W., BARLOGIE, B., RUDIKOFF, S. & SHAUGHNESSY, J. D., JR. 2008. Dkk1-induced inhibition of Wnt signaling in osteoblast differentiation is an underlying mechanism of bone loss in multiple myeloma. *Bone,* 42**,** 669-80.
RAHAL, Z., EL NEMR, S., SINJAB, A., CHAMI, H., TFAYLI, A. & KADARA, H. 2017. Smoking and Lung Cancer: A Geo-Regional Perspective. *Front Oncol,* 7**,** 194.
RATAJCZAK, A. E., SZYMCZAK-TOMCZAK, A., RYCHTER, A. M., ZAWADA, A., DOBROWOLSKA, A. & KRELA-KAZMIERCZAK, I. 2021. Impact of Cigarette Smoking on the Risk of Osteoporosis in Inflammatory Bowel Diseases. *J Clin Med,* 10.
REGAN, J. & LONG, F. 2013. Notch signaling and bone remodeling. *Curr Osteoporos Rep,* 11**,** 126-9.
REUMANN, M. K., SCHAEFER, J., TITZ, B., ASPERA-WERZ, R. H., WONG, E. T., SZOSTAK, J., HÄUSSLING, V., EHNERT, S., LEROY, P., TAN, W. T., KUCZAJ, A., AUDRETSCH, C., SPRINGER, F., BADKE, A., AUGAT, P., QUENTANILLA-FEND, L., MARTELLA, M., LEE, K. M., PEITSCH, M. C., HOENG, J. & NUSSLER, A. K. 2020. E-vapor aerosols do not compromise bone integrity relative to cigarette smoke after 6-month inhalation in an ApoE(-/-) mouse model. *Arch Toxicol,* 94**,** 2163-2177.
RICO-LLANOS, G. A., BORREGO-GONZÁLEZ, S., MONCAYO-DONOSO, M., BECERRA, J. & VISSER, R. 2021. Collagen Type I Biomaterials as Scaffolds for Bone Tissue Engineering. *Polymers (Basel),* 13.
RIDEOUT, K., TESCHKE, K., DIMICH-WARD, H. & KENNEDY, S. 2005. Considering risks to healthcare workers from glutaraldehyde alternatives in high-level disinfection. *Journal of Hospital Infection,* 59**,** 4-11.
ROSEN, V. 2006. BMP and BMP inhibitors in bone. *Ann N Y Acad Sci,* 1068**,** 19-25.
RUAN, Y., KATO, H., TAGUCHI, Y., YAMAUCHI, N. & UMEDA, M. 2021. Irradiation by high-intensity red light-emitting diode enhances human bone

marrow mesenchymal stem cells osteogenic differentiation and mineralization through Wnt/β-catenin signaling pathway. *Lasers Med Sci,* 36**,** 55-65.

RUDE, R. K. & GRUBER, H. E. 2004. Magnesium deficiency and osteoporosis: animal and human observations. *J Nutr Biochem,* 15**,** 710-6.

RUDE, R. K., GRUBER, H. E., WEI, L. Y. & FRAUSTO, A. 2005. Immunolocalization of RANKL is increased and OPG decreased during dietary magnesium deficiency in the rat. *Nutr Metab (Lond),* 2**,** 24.

RUDE, R. K., GRUBER, H. E., WEI, L. Y., FRAUSTO, A. & MILLS, B. G. 2003. Magnesium deficiency: effect on bone and mineral metabolism in the mouse. *Calcif Tissue Int,* 72**,** 32-41.

RUDE, R. K., KIRCHEN, M. E., GRUBER, H. E., MEYER, M. H., LUCK, J. S. & CRAWFORD, D. L. 1999. Magnesium deficiency-induced osteoporosis in the rat: uncoupling of bone formation and bone resorption. *Magnes Res,* 12**,** 257-67.

RUDE, R. K. & OLERICH, M. 1996. Magnesium deficiency: possible role in osteoporosis associated with gluten-sensitive enteropathy. *Osteoporos Int,* 6**,** 453-61.

RUOSS, M., REBHOLZ, S., WEIMER, M., GROM-BAUMGARTEN, C., ATHANASOPULU, K., KEMKEMER, R., KASS, H., EHNERT, S. & NUSSLER, A. K. 2020. Development of Scaffolds with Adjusted Stiffness for Mimicking Disease-Related Alterations of Liver Rigidity. *J Funct Biomater,* 11.

RYAN, G., MAGONY, R., GORTLER, H., GODBOUT, C., SCHEMITSCH, E. H. & NAUTH, A. 2021. Systemically impaired fracture healing in small animal research: A review of fracture repair models. *J Orthop Res,* 39**,** 1359-1367.

SAHIN, E., ORHAN, C., BALCI, T. A., ERTEN, F. & SAHIN, K. 2021. Magnesium Picolinate Improves Bone Formation by Regulation of RANK/RANKL/OPG and BMP-2/Runx2 Signaling Pathways in High-Fat Fed Rats. *Nutrients,* 13.

SAHOTA, S., LOVECCHIO, F., HAROLD, R. E., BEAL, M. D. & MANNING, D. W. 2018. The effect of smoking on thirty-day postoperative complications after total joint arthroplasty: a propensity score-matched analysis. *The Journal of Arthroplasty,* 33**,** 30-35.

SAITO, N., TABATA, N., SAITO, S., ANDOU, Y., ONAGA, Y., IWAMITSU, A., SAKAMOTO, M., HORI, T., SAYAMA, H. & KAWAKITA, T. 2004. Bone mineral density, serum albumin and serum magnesium. *J Am Coll Nutr,* 23**,** 701S-3S.

SALAM, S., GALLAGHER, O., GOSSIEL, F., PAGGIOSI, M., KHWAJA, A. & EASTELL, R. 2018. Diagnostic Accuracy of Biomarkers and Imaging for Bone Turnover in Renal Osteodystrophy. *J Am Soc Nephrol,* 29**,** 1557-1565.

SCHINDELER, A., MCDONALD, M. M., BOKKO, P. & LITTLE, D. G. 2008. Bone remodeling during fracture repair: The cellular picture. *Semin Cell Dev Biol,* 19**,** 459-66.

SCHLICKEWEI, C. W., KLEINERTZ, H., THIESEN, D. M., MADER, K., PRIEMEL, M., FROSCH, K. H. & KELLER, J. 2019. Current and Future Concepts for the Treatment of Impaired Fracture Healing. *Int J Mol Sci,* 20.

SHEEN, J. R. & GARLA, V. V. 2021. Fracture Healing Overview. *StatPearls.* Treasure Island (FL): StatPearls Publishing

SILVA FILHO, S. E., SANDES, C. S., VIEIRA, J. E. & CAVALCANTI, I. L. 2021. Analgesic effect of magnesium sulfate during total intravenous anesthesia: randomized clinical study. *Brazilian Journal of Anesthesiology,* 71**,** 550-557.

SIMS, N. A. & GOOI, J. H. 2008. Bone remodeling: Multiple cellular interactions required for coupling of bone formation and resorption. *Semin Cell Dev Biol,* 19**,** 444-51.

SLOAN, A., HUSSAIN, I., MAQSOOD, M., EREMIN, O. & EL-SHEEMY, M. 2010. The effects of smoking on fracture healing. *Surgeon,* 8**,** 111-6.

SOARES DO AMARAL, N., CRUZ, E. M. N., DE MELO MAIA, B. & MALAGOLI ROCHA, R. 2016. Noncoding RNA Profiles in Tobacco- and Alcohol-Associated Diseases. *Genes (Basel),* 8.

SOLEIMANPOUR, H., IMANI, F., DOLATI, S., SOLEIMANPOUR, M. & SHAHSAVARINIA, K. 2022. Management of pain using magnesium sulphate: A narrative review. *Postgraduate Medicine*.

SPENCER, G. J., UTTING, J. C., ETHERIDGE, S. L., ARNETT, T. R. & GENEVER, P. G. 2006. Wnt signalling in osteoblasts regulates expression of the receptor activator of NFkappaB ligand and inhibits osteoclastogenesis in vitro. *J Cell Sci,* 119**,** 1283-96.

SREEKUMAR, V., ASPERA-WERZ, R., EHNERT, S., STROBEL, J., TENDULKAR, G., HEID, D., SCHREINER, A., ARNSCHEIDT, C. & NUSSLER, A. K. 2018. Resveratrol protects primary cilia integrity of human mesenchymal stem cells from cigarette smoke to improve osteogenic differentiation in vitro. *Arch Toxicol,* 92**,** 1525-1538.

SZCZESNY, G. 2002. Molecular aspects of bone healing and remodeling. *Pol J Pathol,* 53**,** 145-53.

TEITELBAUM, S. L. 2000. Bone resorption by osteoclasts. *Science,* 289**,** 1504-8.

THEIN-HAN, W. W. & MISRA, R. D. 2009. Biomimetic chitosan-nanohydroxyapatite composite scaffolds for bone tissue engineering. *Acta Biomater,* 5**,** 1182-97.

THOMAS, S. & JAGANATHAN, B. G. 2022. Signaling network regulating osteogenesis in mesenchymal stem cells. *J Cell Commun Signal,* 16**,** 47-61.

TISCHLER, E. H., KO, L. M., CHEN, A. F., MALTENFORT, M. G., SCHROEDER, J. & AUSTIN, M. S. 2017. Smoking increases the rate of reoperation for infection within 90 days after primary total joint arthroplasty. *JBJS,* 99**,** 295-304.

TOPRAK, O., TOPUZ, B., MONSEF, Y. A., OTO, C., ORHAN, K. & KARAKECILI, A. 2021. BMP-6 carrying metal organic framework-embedded in bioresorbable electrospun fibers for enhanced bone regeneration. *Mater Sci Eng C Mater Biol Appl,* 120**,** 111738.

TRANQUILLI, A. L., LUCINO, E., GARZETTI, G. G. & ROMANINI, C. 1994. Calcium, phosphorus and magnesium intakes correlate with bone mineral content in postmenopausal women. *Gynecol Endocrinol,* 8**,** 55-8.

TUCKER, K. L., HANNAN, M. T., CHEN, H., CUPPLES, L. A., WILSON, P. W. & KIEL, D. P. 1999. Potassium, magnesium, and fruit and vegetable intakes are associated with greater bone mineral density in elderly men and women. *Am J Clin Nutr,* 69**,** 727-36.

UDAGAWA, N., KOIDE, M., NAKAMURA, M., NAKAMICHI, Y., YAMASHITA, T., UEHARA, S., KOBAYASHI, Y., FURUYA, Y., YASUDA, H., FUKUDA, C. & TSUDA, E. 2021. Osteoclast differentiation by RANKL and OPG signaling pathways. *J Bone Miner Metab,* 39**,** 19-26.

VAN DER TOORN, M., KOSHIBU, K., SCHLAGE, W. K., MAJEED, S., POSPISIL, P., HOENG, J. & PEITSCH, M. C. 2019. Comparison of monoamine oxidase inhibition by cigarettes and modified risk tobacco products. *Toxicol Rep,* 6**,** 1206-1215.

VELILLA, S., GARCIA-MEDINA, J. J., GARCIA-LAYANA, A., DOLZ-MARCO, R., PONS-VAZQUEZ, S., PINAZO-DURAN, M. D., GOMEZ-ULLA, F., AREVALO, J. F., DIAZ-LLOPIS, M. & GALLEGO-PINAZO, R. 2013. Smoking and age-related macular degeneration: review and update. *J Ophthalmol,* 2013**,** 895147.

VERNON, W. B. 1988. The role of magnesium in nucleic-acid and protein metabolism. *Magnesium,* 7**,** 234-48.

WADA, T., NAKASHIMA, T., HIROSHI, N. & PENNINGER, J. M. J. T. I. M. M. 2006. RANKL–RANK signaling in osteoclastogenesis and bone disease. 12**,** 17-25.

WAGNER, J. M., STEUBING, Y., DADRAS, M., WALLNER, C., LOTZIEN, S., HUBER, J., SOGORSKI, A., SACHER, M., REINKEMEIER, F., DITTFELD, S., BECERIKLI, M., LEHNHARDT, M. & BEHR, B. 2022. Wnt3a and ASCs are capable of restoring mineralization in staph aureus-infected primary murine osteoblasts. *J Bone Miner Metab,* 40**,** 20-28.

WALIA, B., LINGENHELD, E., DUONG, L., SANJAY, A. & DRISSI, H. 2018. A novel role for cathepsin K in periosteal osteoclast precursors during fracture repair. *Ann N Y Acad Sci,* 1415**,** 57-68.

WANG, C., CHEN, J. C., XIAO, H. H., KONG, L., ZHAO, Y. M., TIAN, Y., LI, H., TIAN, J. M., CUI, L., WEN, C. M., SHI, Y. J., YANG, J. X. & SHANG, D. J. 2022. Jujuboside A promotes proliferation and neuronal differentiation of APPswe-overexpressing neural stem cells by activating Wnt/β-catenin signaling pathway. *Neurosci Lett***,** 136473.

WANG, J., MA, X. Y., FENG, Y. F., MA, Z. S., MA, T. C., ZHANG, Y., LI, X., WANG, L. & LEI, W. 2017. Magnesium Ions Promote the Biological Behaviour of Rat Calvarial Osteoblasts by Activating the PI3K/Akt Signalling Pathway. *Biol Trace Elem Res,* 179**,** 284-293.

WANG, J., WU, X. & DUAN, Y. 2018. Magnesium Lithospermate B Protects against Lipopolysaccharide-Induced Bone Loss by Inhibiting RANKL/RANK Pathway. *Front Pharmacol,* 9**,** 64.

WANG, W. & YEUNG, K. W. 2017. Bone grafts and biomaterials substitutes for bone defect repair: A review. *Bioactive materials,* 2**,** 224-247.

WANG, X., FRIIS, T. E., MASCI, P. P., CRAWFORD, R. W., LIAO, W. & XIAO, Y. 2016. Alteration of blood clot structures by interleukin-1 beta in association with bone defects healing. *Sci Rep,* 6**,** 35645.

WARBURTON, D. E., NICOL, C. W., GATTO, S. N. & BREDIN, S. S. 2007. Cardiovascular disease and osteoporosis: balancing risk management. *Vasc Health Risk Manag,* 3**,** 673-89.

WEI, J. & KARSENTY, G. 2015. An overview of the metabolic functions of osteocalcin. *Curr Osteoporos Rep,* 13**,** 180-5.

WENG, W., HÄUSSLING, V., ASPERA-WERZ, R. H., SPRINGER, F., RINDERKNECHT, H., BRAUN, B., KÜPER, M. A., NUSSLER, A. K. & EHNERT, S. 2020. Material-Dependent Formation and Degradation of Bone Matrix-Comparison of Two Cryogels. *Bioengineering (Basel),* 7.

WENG, W., ZANETTI, F., BOVARD, D., BRAUN, B., EHNERT, S., UYNUK-OOL, T., HISTING, T., HOENG, J., NUSSLER, A. K. & ASPERA-WERZ, R. H. 2021. A simple method for decellularizing a cell-derived matrix for bone cell cultivation and differentiation. *J Mater Sci Mater Med,* 32**,** 124.

WENG, W., ZANETTI, F., BOVARD, D., BRAUN, B., EHNERT, S., UYNUK-OOL, T., HISTING, T., HOENG, J., NUSSLER, A. K. & ASPERA-WERZ, R. H. 2021. A simple method for decellularizing a cell-derived matrix for bone cell cultivation and differentiation. *Journal of Materials Science: Materials in Medicine,* 32**,** 1-13.

WESTENDORF, J. J., KAHLER, R. A. & SCHROEDER, T. M. 2004. Wnt signaling in osteoblasts and bone diseases. *Gene,* 341**,** 19-39.

WONG, S. A., HU, D. P., SLOCUM, J., LAM, C., NGUYEN, M., MICLAU, T., MARCUCIO, R. S. & BAHNEY, C. S. 2021. Chondrocyte-to-osteoblast transformation in mandibular fracture repair. *Journal of Orthopaedic Research®,* 39**,** 1622-1632.

WU, L., FEYERABEND, F., SCHILLING, A. F., WILLUMEIT-RÖMER, R. & LUTHRINGER, B. J. C. 2015. Effects of extracellular magnesium extract on the proliferation and differentiation of human osteoblasts and osteoclasts in coculture. *Acta Biomater,* 27**,** 294-304.

WU, L., LUTHRINGER, B. J., FEYERABEND, F., SCHILLING, A. F. & WILLUMEIT, R. 2014. Effects of extracellular magnesium on the differentiation and function of human osteoclasts. *Acta biomaterialia,* 10**,** 2843-2854.

WU, W., XIAO, Z., CHEN, Y., DENG, Y., ZENG, D., LIU, Y., HUANG, F., WANG, J., LIU, Y. & BELLANTI, J. A. 2020. CD39 produced from human GMSCs regulates the balance of osteoclasts and osteoblasts through the Wnt/β-catenin pathway in osteoporosis. *Molecular Therapy,* 28**,** 1518-1532.

WU, Y. F., WANG, Y. M., JING, Y. B., ZHUANG, J. P., YAN, J. L., SHAO, Z. K., JIN, M. S., WU, C. J. & ZHOU, Y. 2017. In vivo study of microarc oxidation coated biodegradable magnesium plate to heal bone fracture defect of 3mm width. *Colloids Surf B Biointerfaces,* 158**,** 147-156.

XIAN, C. J., ZHOU, F. H., MCCARTY, R. C. & FOSTER, B. K. 2004.

Intramembranous ossification mechanism for bone bridge formation at the growth plate cartilage injury site. *J Orthop Res,* 22**,** 417-26.

XU, J., HU, X., JIANG, S., WANG, Y., PARUNGAO, R., ZHENG, S., NIE, Y., LIU, T. & SONG, K. 2019. The Application of Multi-Walled Carbon Nanotubes in Bone Tissue Repair Hybrid Scaffolds and the Effect on Cell Growth In Vitro. *Polymers (Basel),* 11.

XU, L., QIAN, Z., WANG, S., WANG, R., PU, X., YANG, B., ZHOU, Q., DU, C., CHEN, Q., FENG, Z., XU, L., ZHU, Z., QIU, Y. & SUN, X. 2022. Galectin-3 Enhances Osteogenic Differentiation of Precursor Cells from Patients with Diffuse Idiopathic Skeletal Hyperostosis Via Wnt/β-catenin Signaling. *J Bone Miner Res*.

XU, X. J., SHEN, L., YANG, Y. P., ZHU, R., SHUAI, B., LI, C. G. & WU, M. X. 2013. Serum β -Catenin Levels Associated with the Ratio of RANKL/OPG in Patients with Postmenopausal Osteoporosis. *Int J Endocrinol,* 2013**,** 534352.

YANG, L., TSANG, K. Y., TANG, H. C., CHAN, D. & CHEAH, K. S. 2014. Hypertrophic chondrocytes can become osteoblasts and osteocytes in endochondral bone formation. *Proc Natl Acad Sci U S A,* 111**,** 12097-102.

YANG, M., HUANG, W., YANG, F., ZHANG, T., WANG, C. & SONG, Y. 2018. Fam83h mutation inhibits the mineralization in ameloblasts by activating Wnt/β-catenin signaling pathway. *Biochem Biophys Res Commun,* 501**,** 206-211.

YARAGANI, A., SUSHUMA, K., GUDURI, V., THIRUMALASETTY, S., VISHNUBHOTLA, G., KANDIKATLA, P. & CHANDU, V. C. 2020. The influence of tobacco consumption on periodontal health: A stratified analysis based on type of tobacco use. *J Family Med Prim Care,* 9**,** 2061-2066.

YIN, Y., TANG, Q., XIE, M., HU, L. & CHEN, L. 2021. Insights into the mechanism of vascular endothelial cells on bone biology. *Bioscience Reports,* 41.

YOON, V., MAALOUF, N. M. & SAKHAEE, K. 2012. The effects of smoking on bone metabolism. *Osteoporos Int,* 23**,** 2081-92.

ZAIDI, M. 2007. Skeletal remodeling in health and disease. *Nat Med,* 13**,** 791-801.

ZEIGER, E., GOLLAPUDI, B. & SPENCER, P. 2005. Genetic toxicity and carcinogenicity studies of glutaraldehyde—a review. *Mutation Research/Reviews in Mutation Research,* 589**,** 136-151.

ZHANG, J., TANG, L., QI, H., ZHAO, Q., LIU, Y. & ZHANG, Y. 2019. Dual Function of Magnesium in Bone Biomineralization. *Adv Healthc Mater,* 8**,** e1901030.

ZHANG, R., BRYSON, T. D., FOGO, G. M., LIAO, J., RAGHUNAYAKULA, S., MATHIEU, J., WIDER, J. M., REN, X., MAHERAS, K. J. & EMAUS, K. J. 2022. Rapid Treatment with Intramuscular Magnesium Sulfate During Cardiopulmonary Resuscitation Does Not Provide Neuroprotection Following Cardiac Arrest. *Molecular neurobiology***,** 1-10.

ZHANG, R., OYAJOBI, B. O., HARRIS, S. E., CHEN, D., TSAO, C., DENG, H. W. & ZHAO, M. 2013. Wnt/β-catenin signaling activates bone morphogenetic protein 2 expression in osteoblasts. *Bone,* 52**,** 145-56.

ZHANG, Z., PAN, X., CHEN, M. & BAI, M. 2022. Wnt signalling in oral and maxillofacial diseases. *Cell Biol Int,* 46**,** 34-45.

ZHANG, Z. H., JIA, X. Y., FANG, J. Y., CHAI, H., HUANG, Q., SHE, C., JIA, P., GENG, C. & XU, W. 2020. Reduction of SOST gene promotes bone formation through the Wnt/β-catenin signalling pathway and compensates particle-induced osteolysis. *J Cell Mol Med,* 24**,** 4233-4244.

ZHAO, D., WITTE, F., LU, F., WANG, J., LI, J. & QIN, L. 2017. Current status on clinical applications of magnesium-based orthopaedic implants: A review from clinical translational perspective. *Biomaterials,* 112**,** 287-302.

ZHOU, X., VON DER MARK, K., HENRY, S., NORTON, W., ADAMS, H. & DE CROMBRUGGHE, B. 2014. Chondrocytes transdifferentiate into osteoblasts in endochondral bone during development, postnatal growth and fracture healing in mice. *PLoS Genet,* 10**,** e1004820.

ZHU, S., HÄUSSLING, V., ASPERA-WERZ, R. H., CHEN, T., BRAUN, B., WENG, W., HISTING, T. & NUSSLER, A. K. 2020. Bisphosphonates Reduce Smoking-Induced Osteoporotic-Like Alterations by Regulating RANKL/OPG in an Osteoblast and Osteoclast Co-Culture Model. *Int J Mol Sci,* 22.

ZHU, S., HÄUSSLING, V., ASPERA-WERZ, R. H., CHEN, T., BRAUN, B., WENG, W., HISTING, T. & NUSSLER, A. K. 2021. Bisphosphonates reduce smoking-induced osteoporotic-like alterations by regulating RANKL/OPG in an osteoblast and osteoclast co-culture model. *International Journal of Molecular Sciences,* 22**,** 53.

ZOCCHI, M., BÉCHET, D., MAZUR, A., MAIER, J. A. & CASTIGLIONI, S. 2021. Magnesium Influences Membrane Fusion during Myogenesis by Modulating Oxidative Stress in C2C12 Myoblasts. *Nutrients,* 13.

8. Declaration

The research was entirely conducted in Siegfried Weller Institute for Trauma Research, Eberhard Karls Universität Tübingen, Tübingen.

Prof. Dr. rer nat. Andreas K. Nüssler, Dr. sc hum. Romina H. Aspera-Werz and I conceptualized the study. Dr. sc hum. Romina H. Aspera-Werz and I conceived and designed the experiments. All experiments were carried out and analyzed by myself.

I declare that all relevant data are our original work, except for the quoted references and figures. Also, one figure from other papers has permission licenses.

I hereby declare that the submitted thesis entitled: “Magnesium supplementation reduces cigarette smoke–associated cell damage in 3D bone fracture healing model” has been written by myself. This work has not been submitted for any other degree. This thesis was linguistically edited by a commercial Professional English Proofreading Service (Proof-Reading-Service.com).

_____

Place/date/signature of doctoral candidate

9. Publication

Results of this thesis were partially used for publication:

- *Title:*

Material-Dependent Formation and Degradation of Bone Matrix-Comparison of Two Cryogels.

Author:

Weng, W., Häussling, V., Aspera-Werz, R. H., Nüssler AK, Ehnert, S.

Journal:

Bioengineering (Basel). Impact score 4.49

- *Title:*

A simple method for decellularizing a cell-derived matrix for bone cell cultivation and differentiation.

Author:

Weng, W., Zanetti, F., Bovard, D., Ehnert, S., Nüssler AK, Aspera-Werz, R. H

Journal:

Journal of Materials Science: Materials in Medicine. IF 3.896

- *Title:*

Tobacco Heating System 2.4 has a reduced impact compared to cigarette smoke on bone metabolism: possible role in fracture healing.

Author:

Weng, W., Zanetti, F., Bovard, D., Ehnert, S., Nüssler AK, Aspera-Werz, R. H

Journal:

Food and Chemical Toxicology (Pending submission). IF 6.023

- *Title:*

Magnesium supplementation reduces cigarette smoke–associated cell damage in 3D bone fracture healing model.

Author:

Weng, W., Ehnert, S., Nüssler AK, Aspera-Werz, R. H

Journal:

Clinical Nutrition (Pending submission). IF 7.324

10. Acknowledgements

I would like to express my appreciation to many individuals who have assisted me during my thesis.

First and foremost, I am grateful to my supervisor, Prof. Dr. rer. nat. Andreas K. Nüssler for guiding me throughout a doctoral thesis at the Siegfried Weller Institute (SWI). There are a variety of things Prof. Dr. rer. nat. Andreas K. Nüssler has taught me, however nothing was more crucial than his motivation and energy to explore the boundaries of knowledge in order to improve the management of orthopedic diseases in smokers. If not for his constructive suggestions and incredible dedication, the achievements mentioned in this thesis would not have been possible.

Aside from my advisor, I would like to acknowledge the kind assistance and help from Dr. sc hum. Romina H. Aspera-Werz. Her passion and excitement for science were contagious, and she always encouraged me to explore new things. Her encouragement, patience and professional instructions have help me work out my problems during my study.

I have a special thanks to PD Dr. sc hum. Sabrina Ehnert, whose comments and suggestions were incredibly valuable for improving my study.

I deeply acknowledge all my colleagues at SWI: Tatiana, Anick, Svetlana, Bianca, Regina, Marie, Victor, Caren, Helen, Marc who have provided me with their useful feedback on my research.

Many thanks to my Chinese colleagues: Tao Chen, Shen Zhu, Zi Li, Huizhi Guo, Chao Lu, Yangmengfan Chen, Chao Liu, and Xiaowei Huang for happy memories in Tübingen.

Last my thanks would go to my beloved family for their loving considerations and great confidence in me during the years.